15 Umetani M, Nakao H, Doi T *et al.* A novel cell adhesion inhibitor, K-7174, reduces the endothelial VCAM-1 induction by inflammatory cytokines, acting through the regulation of GATA. Biochem Biophys Res Commun 2000; **272**:370–4.
16 Delporte C, O'Connell BC, He X *et al.* Increased fluid secretion after adenoviral-mediated transfer of the aquaporin-1 cDNA to irradiated rat salivary glands. Proc Natl Acad Sci USA 1997; **94**:3268–73.
17 White SC, Casarett GW. Induction of experimental autoallergic sialadenitis. J Immunol 1974; **112**:178–85.
18 Mikulowska-Mennis A, Xu B, Berberian JM, Michie SA. Lymphocyte migration to inflamed lacrimal glands is mediated by vascular cell adhesion molecule-1/alpha(4) beta(1) integrin, peripheral node addressin/l-selectin, and lymphocyte function-associated antigen-1 adhesion pathways. Am J Pathol 2001; **159**:671–81.
19 Toda I, Sullivan BD, Rocha EM, Da Silveira LA, Wickham LA. Sullivan DA. Impact of gender on exocrine gland inflammation in mouse models of Sjogren's syndrome. Exp Eye Res 1999; **69**:355–66.
20 Tsubota K, Fujita H, Tadano K *et al.* Improvement of lacrimal function by topical application of CyA in murine models of Sjogren's syndrome. Invest Ophthalmol Vis Sci 2001; **42**:101–10.
21 Kong L, Robinson CP, Peck AB *et al.* Inappropriate apoptosis of salivary and lacrimal gland epithelium of immunodeficient NOD-scid mice. Clin Exp Rheumatol 1998; **16**:675–81.
22 Nakano H, Doi T, Suda M *et al.* An inhibitor of VCAM-1 expression and its implication as a novel treatment of inflammatory diseases. J Atheroscler Thromb 1998; **4**:149–55.
23 Iademarco MF, McQuillan JJ, Rosen GD, Dean DC. Characterization of the promoter for vascular cell adhesion molecule-1 (VCAM-1). J Biol Chem 1992; **267**:16323–9.
24 Neish AS, Read MA, Thanos D, Pine R, Maniatis T, Collins T. Endothelial interferon regulatory factor 1 cooperates with NF-kappa B as a transcriptional activator of vascular cell adhesion molecule 1. Mol Cell Biol 1995; **15**:2558–69.
25 Neish AS, Khachigian LM, Park A, Baichwal VR, Collins T. Sp1 is a component of the cytokine-inducible enhancer in the promoter of vascular cell adhesion molecule-1. J Biol Chem 1995; **270**:28903–9.
26 Lechleitner S, Gille J, Johnson DR, Petzelbauer P. Interferon enhances tumor necrosis factor-induced vascular cell adhesion molecule 1 (CD106) expression in human endothelial cells by an interferon-related factor 1-dependent pathway. J Exp Med 1998; **187**:2023–30.
27 Papi A, Johnston SL. Respiratory epithelial cell expression of vascular cell adhesion molecule-1 and its up-regulation by rhinovirus infection via NF-kappaB and GATA transcription factors. J Biol Chem 1999; **274**:30041–51.
28 Voraberger G, Schafer R, Stratowa C. Cloning of the human gene for intercellular adhesion molecule 1 and analysis of its 5'-regulatory region. Induction by cytokines and phorbol ester. J Immunol 1991; **147**:2777–86.
29 Cybulsky MI, Allan-Motamed M, Collins T. Structure of the murine VCAM1 gene. Genomics 1993; **18**:387–91.
30 Cybulsky MI, Fries JW, Williams AJ *et al.* Gene structure, chromosomal location, and basis for alternative mRNA splicing of the human VCAM1 gene. Proc Natl Acad Sci USA 1991; **88**:7859–63.
31 Saito I, Haruta K, Shimuta M *et al.* Fas ligand-mediated exocrinopathy resembling Sjogren's syndrome in mice transgenic for IL-10. J Immunol 1999; **162**:2488–94.
32 Ishimaru N, Yoneda T, Saegusa K *et al.* Severe destructive autoimmune lesions with aging in murine Sjogren's syndrome through Fas-mediated apoptosis. Am J Pathol 2000; **156**:1557–64.
33 Fox RI. Sjogren's syndrome: immunobiology of exocrine gland dysfunction. Adv Dent Res 1996; **10**:35–40.
34 Tsubota K, Saito I, Miyasaka N. Expression of granzyme A and perforin in lacrimal gland of Sjogren's syndrome. Adv Exp Med Biol 1994; **350**:637–40.
35 Yednock TA, Cannon C, Fritz LC, Sanchez-Madrid F, Steinman L, Karin N. Prevention of experimental autoimmune encephalomyelitis by antibodies against alpha 4 beta 1 integrin. Nature 1992; **356**:63–6.
36 Merrill JE, Benveniste EN. Cytokines in inflammatory brain lesions: helpful and harmful. Trends Neurosci 1996; **19**:331–8.
37 Rice GP, Hartung HP, Calabresi PA. Anti-alpha4 integrin therapy for multiple sclerosis: mechanisms and rationale. Neurology 2005; **64**:1336–42.
38 Carter RA, Campbell IK, O'Donnel KL, Wicks IP. Vascular cell adhesion molecule-1 (VCAM-1) blockade in collagen-induced arthritis reduces joint involvement and alters B cell trafficking. Clin Exp Immunol 2002; **128**:44–51.
39 Singh J, Van Vlijmen H, Liao Y *et al.* Identification of potent and novel alpha4beta1 antagonists using in silico screening. J Med Chem 2002; **45**:2988–93.
40 Foster CA. VCAM-1/alpha 4-integrin adhesion pathway: therapeutic target for allergic inflammatory disorders. J Allergy Clin Immunol 1996; **98**:S270–7.

Research Paper

Journal of Vascular Research

J Vasc Res 2007;44:138–148
DOI: 10.1159/000098520

Received: February 16, 2006
Accepted after revision: November 19, 2006
Published online: January 11, 2007

Functional Analysis of an Established Mouse Vascular Endothelial Cell Line

Tatsuaki Nishiyama[a, b] Kenji Mishima[a] Fumio Ide[a] Koichi Yamada[a]
Kumi Obara[a] Aki Sato[a] Noriko Hitosugi[a] Hiroko Inoue[a] Kazuo Tsubota[b, c]
Ichiro Saito[a, b]

[a]Department of Pathology, Tsurumi University School of Dental Medicine, Yokohama;
[b]Sjögren's Syndrome Project, Shinanomachi Research Park, and [c]Department of Ophthalmology,
Keio University School of Medicine, Tokyo, Japan

Key Words
Cellular binding · Endothelial cell line · p53-deficient mice · Tube formation

Abstract
Background: In vitro studies using cell lines are useful for the understanding of cellular mechanisms. The purpose of our study is to develop a new immortalized aortic vascular endothelial cell (EC) line that retains endothelial characteristics and can facilitate the study of ECs. ***Methods:*** A mouse aortic vascular EC line (MAEC) was established from p53-deficient mouse aorta and cultured for over 100 passages. The expression of endothelial markers was assessed, and the function of this cell line was analyzed by tube formation and binding assays. ***Results:*** MAEC retained many endothelial properties such as cobblestone appearance, contact-inhibited growth, active uptake of acetylated low-density lipoprotein, existence of Weibel-Palade bodies and several EC markers. MAECs exhibited tube formation activity both in vitro and in vivo. Furthermore, crucially, tumor necrosis factor α, an inflammatory cytokine, promoted lymphocyte adhesion to MAECs, suggesting that MAECs may facilitate the study of atherosclerosis and local inflammatory reactions in vitro. ***Conclusion:*** We describe the morphological and cell biological characteristics of MAEC, providing strong evidence that it retained endothelial properties. This novel cell line can be a useful tool for studying the biology of ECs.

This work was partially supported by grants-in-aid for scientific research from the Ministry of Education, Culture, Sports, Science and Technology of Japan.

Introduction

Endothelial cells (ECs) line the inner surface of blood and lymphatic vessels and play critical roles in vasculogenesis, angiogenesis, the development and remodeling of the vasculature, vascular permeability and circulation [1]. In vitro studies using EC lines or primary ECs are highly useful to understand the mechanisms of the results gained from in vivo analyses. The development of techniques for the isolation and growth of ECs in vitro [2] has resulted in a dramatic increase in our understanding of endothelial function. For human studies, a number of in vitro experimental EC models have been developed using human umbilical vein ECs (HUVECs) [3, 4]. For

KARGER
Fax +41 61 306 12 34
E-Mail karger@karger.ch
www.karger.com

1018–1172/07/0442–0138$23.50/0

Accessible online at:
www.karger.com/jvr

Dr. Ichiro Saito
Department of Pathology, Tsurumi University School of Dental Medicine
2-1-3 Tsurumi, Tsurumi-ku
Yokohama, 230-8501 (Japan)
Tel. +81 45 580 8360, Fax +81 45 572 2888, E-Mail saito-i@tsurumi-u.ac.jp

mouse studies, ECs have been isolated from murine lung [5], lymph nodes [6], and brain [7]. However, the isolation of primary ECs from mouse organs is both time consuming and costly, and the ECs of some organs can only be passaged two or three times before significant senescence occurs [8]. These problems can be overcome by the use of immortalized cell lines because they show stable proliferation and clonality. Numerous attempts have been made by researchers to establish mouse EC lines. Although several mouse and rat EC lines have been established, the immortalization resulted in phenotypic changes, such as a decrease in surface antigens [9] and tube-forming activity [10], and less responsiveness to cytokines [11]. Considering these reports, immortalized EC lines retaining the differentiated characteristics of the original tissues are useful materials for the study of EC proliferation, differentiation, and metabolism. In addition, no aortic EC lines have been described previously.

Gene transfer of simian virus 40 (SV40) T antigen is frequently used for cell immortalization, and some cell lines immortalized by SV40 T antigen-encoding transgenes have proven useful in studies on the regulation of gene expression [12]. However, present disadvantages of SV40 vectors are the possible risks related to random integration of the viral genome into the host genome. On the other hand, p53-deficient mice used in this study have only one mutation in the p53 gene. In addition, the DNA content of homozygous cells, which remained in the diploid range, had no chromosomal aberrations [13].

The p53 gene is thought to regulate the process of the cell cycle to induce cell arrest and cell death in normal cells, and the deletion of this gene has been used for cell immortalization. Some cell lines established from p53-deficient mice have been reported, including an osteoblast cell line [14], a pulmonary alveolar type II cell line [15], a prostatic cell line [16], a cerebellar cell line [17], and an astrocyte cell line [18]. Furthermore, an established colon epithelial line did not form colonies in soft agar and was non-tumorigenic in SCID mice [19]. These reports indicate that p53-deficiency is sufficient for immortalization of cells and that the loss of p53 itself does not cause the acquisition of malignant properties. Thus p53-deficient mice are useful for establishing cell lines.

The purpose of our present study is to develop a mouse aortic vascular EC line (MAEC) derived from p53-deficient mouse aorta, and to demonstrate the utility of this cell line in functional assays. We here describe the cell-biological characteristics and function of the MAEC, thus enhancing our understanding of the role of ECs.

Methods

Mice

All animal experimental protocols were approved by the Tsurumi University Ethics Committee. The p53-deficient mice were provided by Dr. Shinichi Aizawa (RIKEN, Tsukuba, Japan). Characterization of the p53-deficient mice has been reported in detail previously [13].

Establishment of Cell Lines from p53-Deficient Mice and Cell Culture

Vascular ECs were prepared as described previously [20] with some modifications. Aorta was harvested from an 8-week-old, female, p53-deficient mouse, minced into 1-mm^2 pieces, washed in Hanks' balanced salt solution without Ca^{2+} and Mg^{2+} (Sigma, St. Louis, Mo., USA), and incubated in a 60-mm dish containing 0.76 mg/ml EDTA, 4.9 mg/ml L-ascorbic acid, and 4.9 mg/ml glutathione at 37°C for 15 min. The minced tissue was washed with soybean trypsin inhibitor (Sigma)/Dulbecco's modified Eagle's medium (DMEM; Sigma) and digested in a mixture of collagenase (type I: 750 U/ml, Wako, Osaka, Japan) and hyaluronidase (type IV: 500 U/ml, Sigma) dissolved in DMEM/F12 (Sigma) containing 10% fetal bovine serum (FBS; BioWhittaker, Walkersville, Md., USA). The first digest suspension was passed through a sterile 100-μm nylon mesh filter, redigested for 2 h using the same digestion procedure, and then passed again through a 100-μm nylon mesh filter. The growth medium employed in this study was M199 medium (Sigma) with 5 ng/ml of recombinant vascular endothelial growth factor (VEGF; Sigma), Hepes (Invitrogen, Carlsbad, Calif., USA), heparin sodium (Shimizu, Shizuoka, Japan) and 5% FBS. HUVECs were cultured in EGM-2 SingleQuots (Cambrex Bio Science Walkersville, Walkersville, Md., USA) and mouse fibroblast cell line (NIH3T3) was cultured in DMEM with 10% FBS. Cells were cultured in humidified incubators at 37°C in an atmosphere of 5% CO_2 and 95% air, and the medium was exchanged every 2–3 days.

DiI-Ac-LDL Uptake Study

MAECs, HUVECs and NIH3T3 cells grown in dishes were incubated for 4 h at 37°C with complete medium containing 10 μg/ml of DiI-Ac-LDL (Biogenesis, Poole, UK). After removal of the medium, the cells were washed three times with PBS and visualized using fluorescent microscopy (Olympus, Melville, N.Y., USA) or analyzed by flow cytometry (Becton Dickinson, Franklin Lakes, N.J., USA).

Flow-Cytometric Analysis

The cultured MAECs were dissociated by treatment with cell dissociation solution (Sigma), harvested by centrifugation and stained with fluorescein isothiocyanate (FITC) conjugated *Griffonia simplicifolia* isolectin B4 (GSLI-B4; Vector Laboratories, Peterborough, UK) and then analyzed by flow cytometry. The cells that took up DiI-Ac-LDL as described above were also monitored and sorted by flow cytometry. Expression of vascular cell adhesion molecule-1 (VCAM-1) on MAECs and very late antigen-4 (VLA-4) on a murine myelomonocytic leukemia cell line (WEHI-3B) was also analyzed by flow cytometry using anti-mouse VCAM-1 antibody, anti-mouse VLA-4 antibody and anti-rat IgG FITC conjugate (Santa Cruz Biotechnology, Santa Cruz, Calif., USA).

Ultrastructural Examination by Transmission Electron Microscopy

MAECs cultured in plastic dishes were washed in PBS and then fixed in 2.5% glutaraldehyde. After fixation in 1% osmium tetroxide, they were embedded in Epon 812. Ultrathin sections were cut by an LKB ultramicrotome, stained with uranyl acetate and lead citrate and examined using a Hitachi H-500 electron microscope.

RT-PCR Assay

Total RNA was extracted from MAECs, HUVECs, NIH3T3 and the aorta of a C57BL/6 mouse, with TRIzol reagent (Life Technologies, Rockville, Md., USA), and cDNA was prepared from RNA with 50 pmol of random hexamer and 200 U of reverse transcriptase (Invitrogen, Carlsbad, Calif., USA); 0.5 μl of a 20-μl cDNA mixture was used for PCR with 5 pmol each of forward and reverse primers and 2.5 U of Ex Taq DNA polymerase (Takara Shuzo, Kyoto, Japan). The sequences of the specific sense and antisense oligonucleotide primer pairs were as follows: VEGF receptor-2 (Flk-1), TGGCAGCACGAAACATTCT and TTGCAGGAGGTTTCCCAAAT; von Willebrand factor (vWf), TCCCAGACCATCAGCCCT and GGTAAAGGTGGGTCTGCATT; β-actin, CTCTTTGATGTCACGCACGATTTC and GTGGGCCGCTCTAGGCACCAA; intercellular adhesion molecule-2 (ICAM-2), TGCTGGAGCCTGTCTCTTCTT and TTTCCCGAACACGTGAAATG; Tie-2, TATTGAGTATGCCCCGCATG and GCTAACAATCTCCCAGAGCAA; endothelial nitric oxide synthase (eNOS) for mice, AAAGAATTGGGAAGTGGGCA and AACATTTCCTGTGCAGTCCTG, and eNOS for humans, GACGCTACGAGGAGTGGAAG and TAGGTCTTGGGGTTGTCAGG.

Samples were amplified through 35 cycles at an annealing temperature of 52°C in a PCR Thermal Cycler (Applied Biosystems, Foster City, Calif., USA).

Immunofluorescence Staining

Cytospin (Thermo Electron, Waltham, Mass., USA) preparations of MAECs were fixed in 3% (v/v) paraformaldehyde at room temperature for 15 min and blocked in DAKO Cytomation Protein Block Serum-Free Ready-to-use (DAKO, Glostrup, Denmark) for 1 h. Cells were incubated with primary antibodies, such as phycoerythrin-conjugated anti-Flk-1 monoclonal antibody (Pharmingen, San Diego, Calif., USA), anti-vascular endothelial (VE)-cadherin monoclonal antibody (Pharmingen), anti-vWf monoclonal antibody (DAKO) or ICAM-2 monoclonal antibody (Pharmingen) at 4°C overnight. As a control, isotype control (R & D Systems, Minneapolis, Minn., USA) was used as a primary antibody. After washing with cold PBS, the cells were incubated with biotin-conjugated anti-rat IgG (Chemicon, Temecula, Calif., USA) or biotin-conjugated anti-mouse IgG (Chemicon) at 4°C for 1 h. Subsequently, the cells were incubated with FITC-conjugated streptavidin (BD Biosciences, San Jose, Calif., USA) at 4°C for 1 h. Preparations were mounted in DAKO fluorescent mounting medium (DAKO) and viewed under a fluorescence microscope (TS100; Nikon, Tokyo, Japan).

Immunoblotting

The proteins obtained from MAECs and homogenized uterus were boiled in sample buffer (500 mM Tris-HCl, pH 6.8, 4% SDS, 20% glycerol, and 2% mercaptoethanol) for 5 min. Equal amounts of total protein were loaded on each lane and run on SDS-PAGE, followed by electrophoretic transfer of the proteins to polyvinylidene difluoride membrane. Membranes were first blocked with 5% skim milk for 1 h and then incubated with the mouse anti-α smooth muscle actin (α-SMA) monoclonal antibody (Research Diagnostics, Flanders, N.J., USA) or anti-tubulin monoclonal antibody (Sigma) for 1 h. After three sequential 5-min washes with washing buffer (20 mM Tris-HCl, pH 7.4, and 0.1% Tween 20), the membranes were incubated with anti-rabbit IgG or anti-mouse IgG peroxidase-conjugated secondary antibodies (Santa Cruz Biotechnology) for 1 h at room temperature and then again washed as described above. Bound protein was developed with ECL detection reagents (Amersham Biosciences, Piscataway, N.J., USA) and exposed to X-ray films for 5 s.

Transient Transfection Procedure

1.5×10^5 HUVECs and MAECs were grown on 12-well plates and transiently transfected with pcDNA™ 3.1/*myc*-His/*lacZ* (Invitrogen) using the Lipofectamine™ 2000 Transfection Reagent (Invitrogen), according to the manufacturer's protocol. For measuring transfection efficiency, transiently transfected cells were stained with a β-Gal staining set (Roche, Penzberg, Germany), and positive staining cells were counted by microscopy.

Tube Formation Assay

One hundred microliters of Matrigel (BD Biosciences) were added to 24-well culture plates (Becton Dickinson) and allowed to solidify at 37°C for 30 min. MAECs (2×10^4 cells/well) were seeded on the Matrigel and cultured in M199 medium at 37°C in a humidified atmosphere of 5% CO_2 air. After incubation for 24 h, tube formation was observed using phase-contrast microscopy and photographed.

Infection of Cells with Adenovirus

MAECs (1×10^6) were plated in 100-mm dishes, cultured overnight and incubated with 100 multiplicities of infection of recombinant adenovirus encoding *Escherichia coli* β-galactosidase (Ad-β-gal) for 1 h. Cultured medium was added and MAECs were maintained for 24 h. The recovered MAECs were used for the Matrigel plug assay described below.

In vivo Matrigel Plug Assay

Tube formation activity in vivo was assessed with the Matrigel plug assay. MAECs (2×10^6) were mixed with 0.2 ml of PBS or 0.2 ml of Matrigel and inoculated subcutaneously in 4 nude mice. Matrigel plugs were surgically removed 2 weeks after injection. Each plug was fixed with 10% (vol/vol) formaldehyde, embedded in paraffin, sectioned, and stained with hematoxylin/eosin. For β-gal staining, the removed plugs were then embedded in OCT and frozen with liquid nitrogen. Cryostat sections (5 μm) were made, and the slides were stained for β-gal activity. The slides were then fixed in PBS (pH 7.2) containing 0.25% glutaraldehyde for 10 min at 4°C and stained in 5 mM $K_4Fe(CN)_6 \cdot 3H_2O$, 5 mM $K_3Fe(CN)_6$, 0.2 mM $MgCl_2$, and 1 mg of X-Gal/ml in PBS (pH 7.2) overnight at 37°C. The sections were rinsed in PBS (pH 7.2) and stained with hematoxylin at room temperature for better visualization of the staining.

Cellular Binding Assay

MAECs (2.5×10^4) were seeded into each well of 96-well culture plates (Becton Dickinson). Confluent cultures of MAECs

were stimulated with TNFα (10 ng/ml). WEHI-3B cells (1×10^5) labeled with PKH2 (Sigma) were added to each well and incubated with MAECs for 1 h. Cells that nonspecifically bound to MAECs were removed by inverting the plates for 30 min. Wells were subsequently washed once with serum-free RPMI 1640 (Sigma), and the remaining cells were lysed with 1% Triton X-100 (Sigma). Fluorescence intensity in cell lysate was measured using an automated microplate fluorometer (Perkin Elmer, Wellesley, Mass., USA) at 490 nm. Data are expressed as the percentage of input cells bound.

Nitrate Measurement

Nitrate accumulation was determined by mixing equal volumes of cell culture medium and Griess reagent (Griess Reagent System, Promega, Madison, Wisc., USA) with absorbance at 540 nm on a microplate reader. Standard curves were constructed with known concentrations of $NaNO_2$.

Results

Isolation of Cell Lines from a p53-Deficient Mouse

Cells isolated from the p53-deficient mouse aorta were cultured with M199 medium containing 5 ng/ml recombinant mouse VEGF. Most of the growing cells were morphologically fibroblastic. The cells that showed active uptake of DiI-Ac-LDL were sorted by flow cytometry. After sorting, the collected cells continued to grow, whereas the population of fibroblastic cells diminished. In order to obtain monoclonal cell lines, the sorted cells were subjected to limiting dilution and one of the clones, No. 12, was used for further experiments. This chosen MAEC clone was serially cultured over 1 year and for more than 100 passages. The proliferation of MAECs was examined and the doubling time was 23.2 h. Active uptake of DiI-Ac-LDL of the No. 12 clone was confirmed by flow cytometry (fig. 1c) and confocal microscopy (data not shown). HUVECs clearly showed active uptake of Ac-LDL (fig. 1b), while NIH3T3 showed no uptake (fig. 1d). As active uptake of Ac-LDL is one of the well-known characteristics of ECs, these observations confirmed that MAECs retained characteristics similar to HUVECs and originated in ECs. The MAECs showed typical endothelial morphology, such as cobblestone appearance and contact-inhibited growth (fig. 1a).

Endothelial Characteristics

To investigate whether MAECs had endothelial properties, their characteristics were examined by electron microscopy. As shown in figure 2, Weibel-Palade (WP) bodies were observed in the cytoplasm [21]. WP bodies are abundant within ECs and consist of P-selectin and vWf, formerly designated factor-VIII-related antigen.

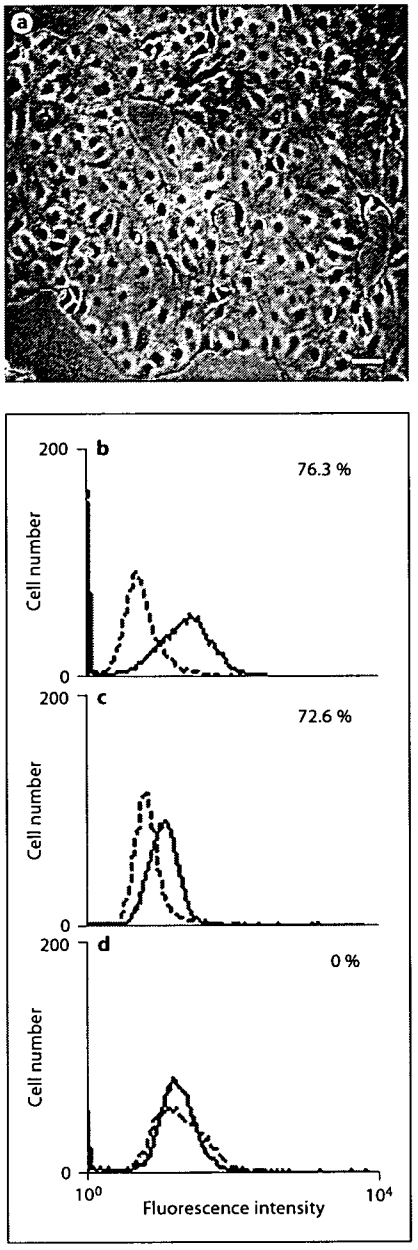

Fig. 1. Establishment and morphology of MAECs. **a** MAECs imaged under phase contrast microscopy. Cells were cultured at 37°C in M199 medium and formed cobblestone morphology with contact-inhibited growth at confluence (magnification ×400, scale bar = 50 μm). Active DiI-Ac-LDL uptake examined by flow cytometry in HUVECs as a positive control (**b**), and MAECs (**c**) and NIH3T3 as a negative control (**d**). Dotted line indicates negative controls without DiI-Ac-LDL.

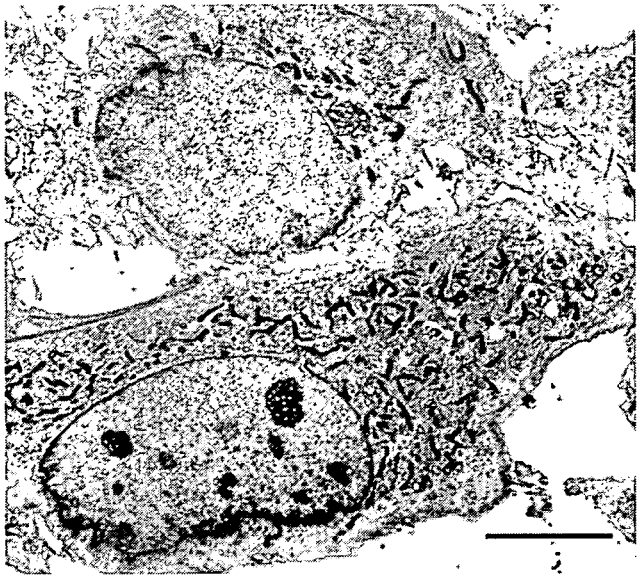

Fig. 2. Presence of WP bodies in MAECs detected by electron microscopy. Many WP bodies are recognized in the cell cytoplasm. P-selectin and vWf are stored in these cytoplasmic components, and the existence of WP bodies indicates that MAECs are ECs (magnification ×1,500, scale bar = 1 μm).

As large blood vessels, like the aorta, are surrounded by smooth muscle cells, we analyzed the possibility of smooth muscle cell contamination. α-SMA, which is a differentiated smooth muscle marker, was not revealed by immunoblotting on MAECs (fig. 3a). However, it was strongly detected in the homogenized uterus, indicating that MAECs were not contaminated by smooth muscle cells.

We next characterized their vasculogenic potential by analyzing the expression of endothelial-specific genes. MAECs were cultured at subconfluent density, and RNA was extracted for analysis of endothelial-related gene expression using RT-PCR. Expression of EC adhesion molecules such as ICAM-2 [22] and growth factor receptors such as VEGFR-2/Flk-1/KDR [23], Tie-2, and vWf [24] were detected in the aorta and MAECs but not in NIH3T3 (fig. 3b). Although the expression level was weaker than normal ECs, the expression profile of endothelial markers in MAECs was similar to that of the aorta. In order to study protein expression, MAECs were prepared by cytospin and subjected to immunofluorescence staining which demonstrated that Flk-1 (fig. 3c), VE-cadherin (fig. 3d), ICAM-2 (fig. 3e) and vWf (fig. 3f) were expressed on MAECs. These results showed that MAECs have various endothelial markers on their surfaces. Especially VE-cadherin, an endothelial-specific cadherin also known as cadherin-5, mediates cell-cell interactions through the formation of an adherence junction, which is important in maintaining vascular integrity [25]. Furthermore, GSLI-B4, which is reported to bind specifically to mouse ECs, bound to MAECs. This binding was visualized with fluorescent microscopy (fig. 3h) and assessed with flow cytometry (data not shown).

For more detailed characterization of the established cell line, transfection efficiency was determined with a liposomal transfection agent. LacZ gene was transfected to MAEC or COS-7, and the transfection efficiency was analyzed by β-gal staining. 13.5% of MAEC were stained and 58.1% of COS-7 were stained under the same conditions. These results demonstrated that MAEC can be transfected, but its efficiency is not high.

Three-Dimensional Culture of ECs in vitro and in vivo

As described above, MAECs retained the morphology and cell surface markers of ECs, and so we performed functional analysis of MAECs as ECs. One of the endothelial functions of this cell line was determined by culture on Matrigel, an extracellular matrix basement membrane that can be used to promote differentiation of ECs [26]. Most ECs rapidly organize and form tube-like structures after plating on Matrigel, and the ability to form tube-like structures on Matrigel can distinguish ECs from common contaminated cell types [5]. MAECs spontaneously reorganized tube-like structures on Matrigel after 24 h (fig. 4a), and they maintained these structures for 3 days. We studied their behavior in vivo to investigate the capacity of MAECs to participate in the process of neovascularization. We used a tumor transplantation model in athymic nude mice. The mixture of MAECs and Matrigel was subcutaneously injected into 4 mice. Athymic nude mice injected with MAECs and PBS served as a control group. Two weeks after injection, MAECs with Matrigel were removed from the mice. The sections of MAECs and Matrigel were stained with HE, and tube-like structures were microscopically detected (fig. 4b). In addition, in order to confirm whether these tube-like structures were constructed of injected MAECs and not recipient ECs, MAECs were labeled with Ad-β-gal prior to injection; thus, the expression of the *E. coli* β-gal gene was directed to the nuclear compartment. One week after injection, MAECs were removed and β-gal activity was analyzed in the frozen sections. Positive staining for β-gal was detected in the tube-like structures, therefore they were disclosed as injected MAECs (fig. 4c). These results indicate that MAECs have the capacity to form three-dimensional structures in vivo.

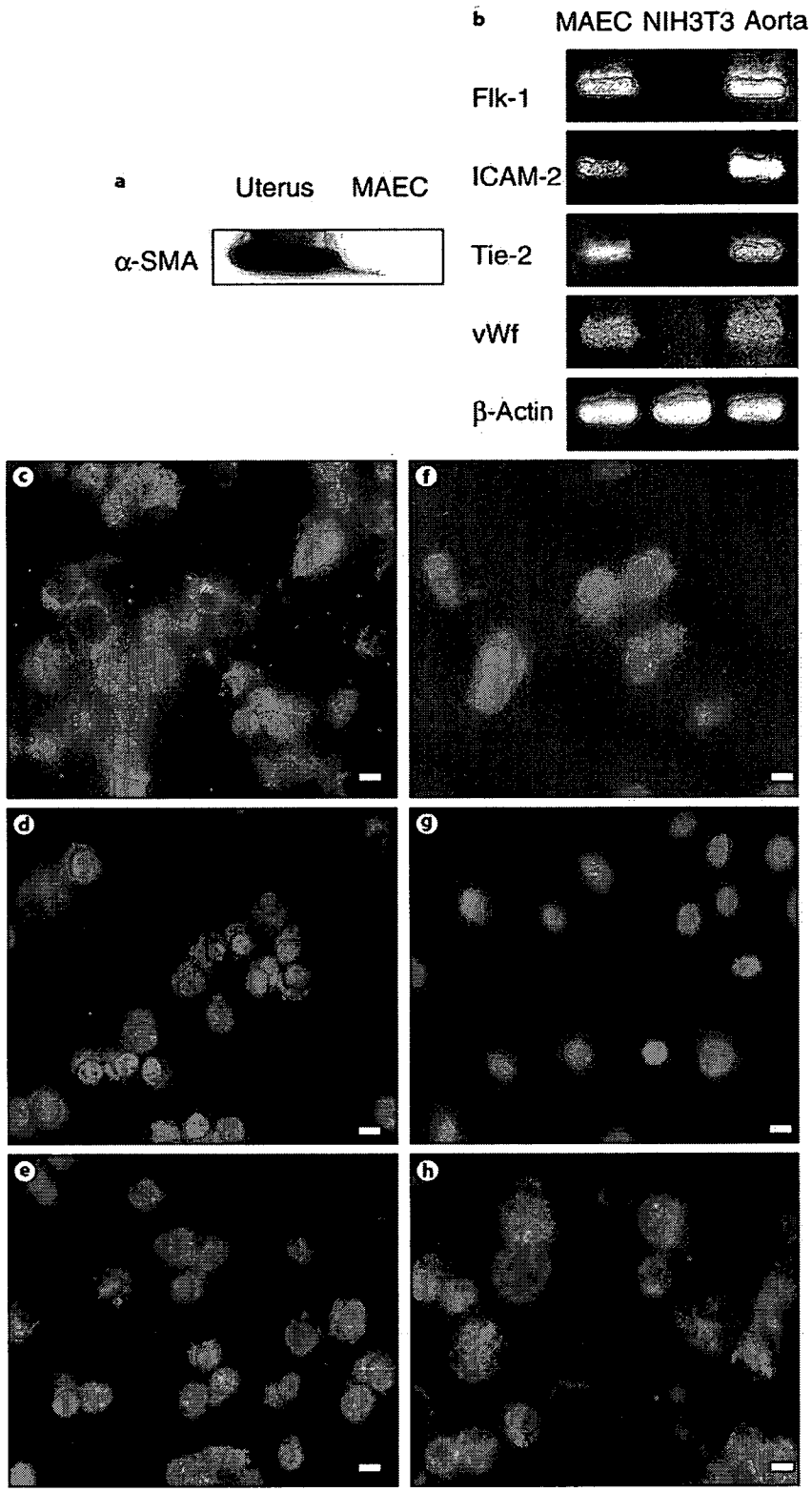

Fig. 3. Endothelial gene expression in MAECs. **a** Western blotting demonstrated that α-SMA was not expressed in MAECs. The uterus was used as a positive control. **b** RT-PCR analysis showed that Flk-1, ICAM-2, Tie-2, and vWf were expressed in MAECs but not in NIH3T3. The aorta was used as a positive control. Expression of Flk-1 (**c**), VE-cadherin (**d**), ICAM-2 (**e**), and vWf (**f**) was monitored by fluorescent microscopy. **g** Isotype control. **h** MAECs showed binding to GSLI-B4 by fluorescent microscopy (magnification ×400, scale bar = 10 μm).

Cellular Binding Activity of MAECs

To assess another endothelial function, cellular binding activity with lymphocytic cells, an in vitro cellular binding assay was performed using TNFα-stimulated MAECs and WEHI-3B cells. TNFα upregulated the expression of VCAM-1 on MAECs (fig. 5a). WEHI-3B cells expressed VLA-4, which is a ligand of VCAM-1, on their surfaces spontaneously (fig. 5b). MAECs were stimulated with 10 ng/ml TNFα and cocultured with WEHI-3B cells for 1 h. After washing, the cells which bound to the MAECs were examined with phase contrast microscopy. Figure 5c shows that cellular binding between WEHI-3B cells and TNFα-stimulated MAECs was enhanced compared with unstimulated MAECs (fig. 5d). This result indicates that TNFα-induced VCAM-1 may play a role in the binding with WEHI-3B cells via VLA-4. For quantification of the binding capacity, WEHI-3B cells labeled with PKH2 were added to MAECs and the binding of these cells was revealed by fluorescence intensity. Although 15.2% of the WEHI-3B cells bound to TNFα-stimulated MAECs, only 3.8% of WEHI-3B cells bound to unstimulated MAECs. As shown in figure 5f, the adhesion of WEHI-3B cells to TNFα-stimulated MAECs was significantly upregulated (* $p = 0.04$, stimulated vs. unstimulated MAECs, Scheffe's test).

NO Production and eNOS Expression in MAECs

Another endothelial function was evaluated: NO production and the expression of eNOS. NO accumulated in HUVEC cultured for 48 h, but little NO was detected in the MAEC culture (fig. 5g), and 100 ng/ml of VEGF did not upregulate NO production. eNOS expression was detected in MAECs by RT-PCR but not in the mouse fibroblast cell line, NIH3T3 cells (fig. 5g). This expression was weaker than that in HUVECs as well as the other endothelial markers described above. eNOS expression of MAECs may decrease during the immortalization process and it may result in low level NO production.

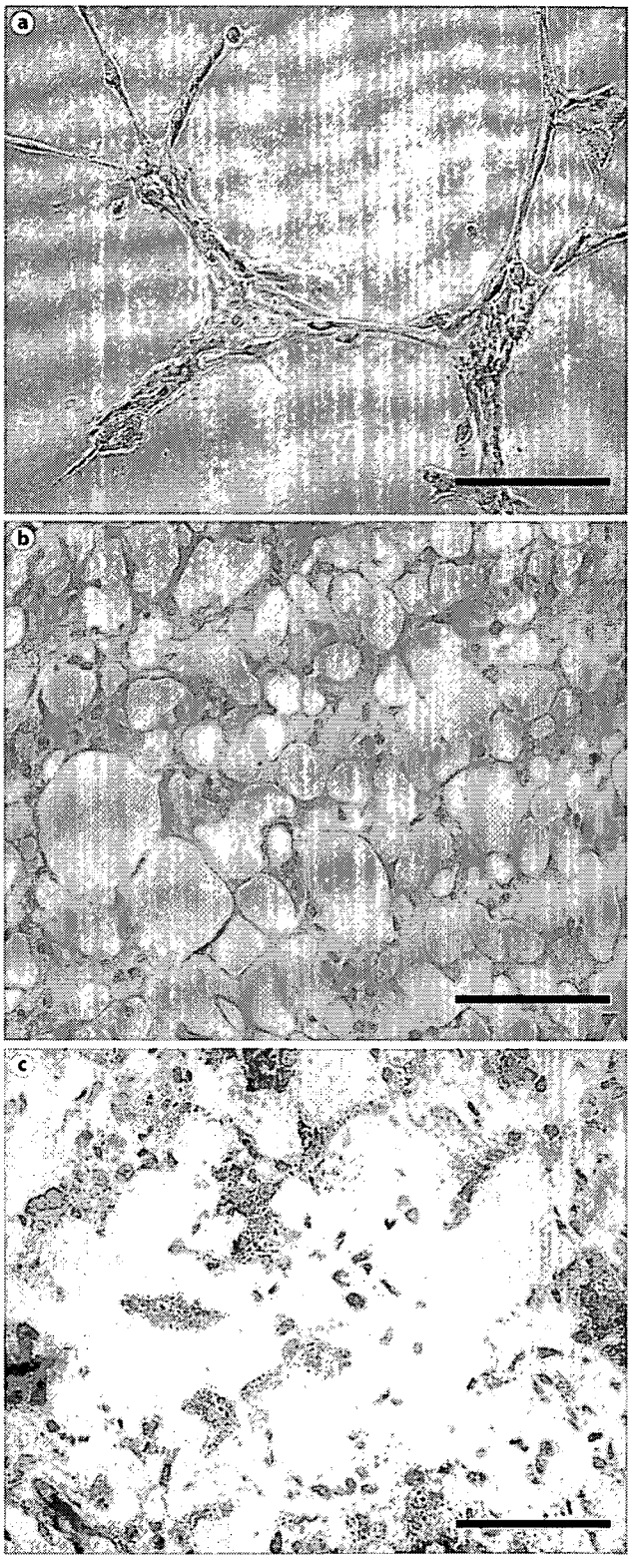

Fig. 4. Tube formation of MAECs on Matrigel and in vivo. **a** Tube formation by MAECs 24 h after seeding the cells on Matrigel (magnification ×200, scale bar = 100 μm). **b** MAECs and Matrigel were inoculated into nude mice, and removed mixtures were sectioned and analyzed by HE staining. Many tube formations were seen in the section. **c** MAECs that were transfected with Ad-β-gal were inoculated and analyzed. β-gal-labeled MAECs were seen in the sections. **b**, **c** Magnification ×400, scale bar = 50 μm.

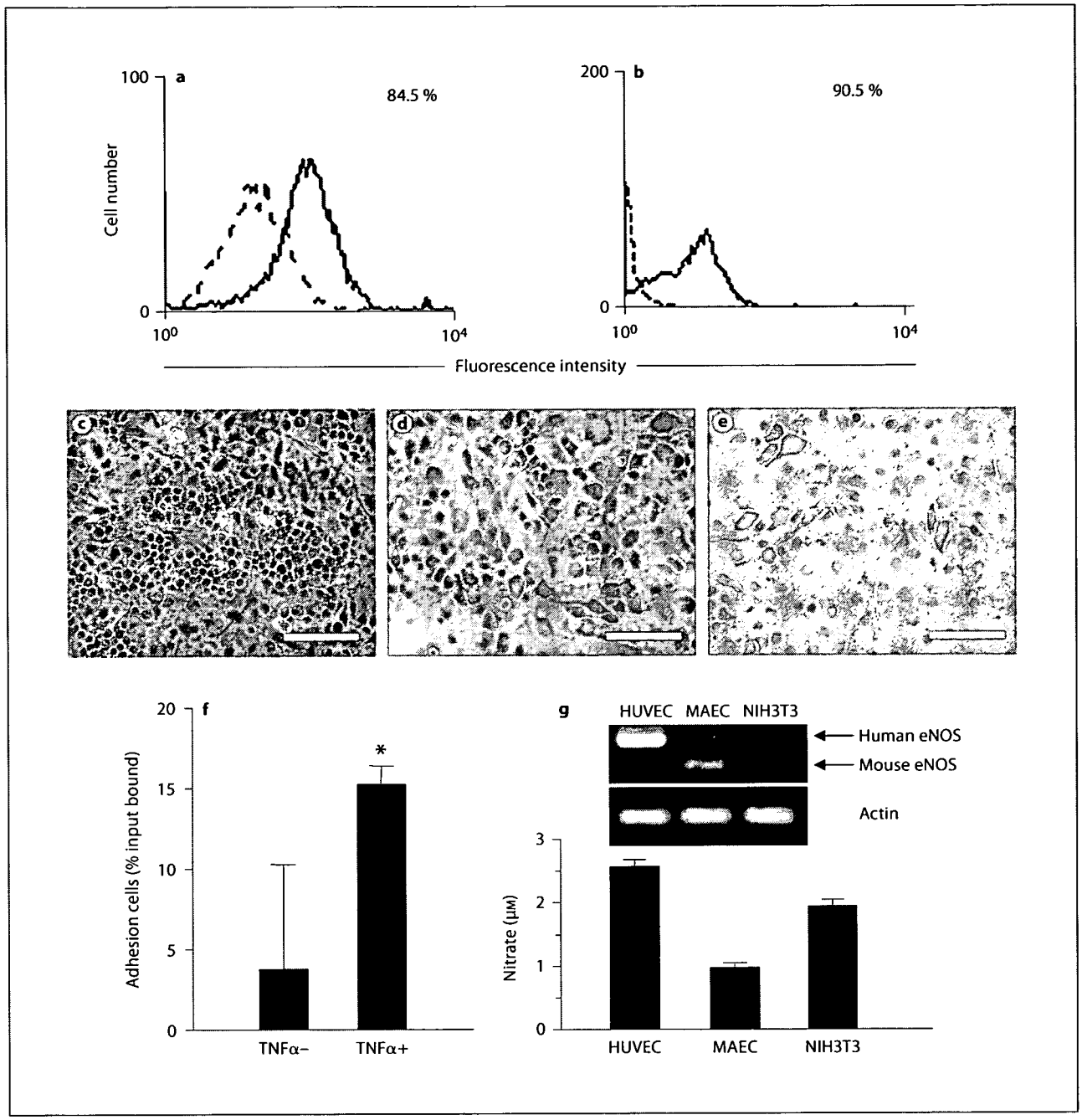

Fig. 5. a Representative histograms depict the isotype control (dotted line) and stimulated endothelial VCAM-1 expression after incubation with TNFα (10 ng/ml) for 4 h. **b** Surface expression of VLA-4 on WEHI-3B. The dotted line shows the isotype control. The data of phase contrast microscopy show cellular binding between WEHI-3B cells and TNFα-stimulated MAECs (**c**) or unstimulated MAECs (**d**). **e** The control with no WEHI-3B cells. **c–e** Magnification ×200, scale bar = 100 μm. **f** Cellular binding activity of MAECs to mononuclear cells was measured by cellular binding (* $p = 0.04$). **g** The expression of eNOS by RT-PCR and nitrate production in MAEC. **f, g** The results are representative of several experiments.

Discussion

In order to understand the mechanism of events shown in in vivo analysis, it is important to reconstruct them in in vitro experiments. HUVECs contributed to these in vitro analyses for human EC biology. For in vivo experiments using mice, some mouse EC lines were previously reported [27–30], and these cell lines each had endothelial-like characteristics and were useful to some degree. Although Su et al. [30] showed tube formation of their cell line on Matrigel, no other EC functions were reported in their studies. A cell line that retains as many similar functions to normal ECs as possible is required for various in vitro analyses. In our present study, we assessed the characteristics and functions of the newly established EC line, MAECs. MAECs exhibited typical and basic criteria for the identification of ECs [31], e.g. cobblestone appearance, contact-inhibited growth and active uptake of DiI-Ac-LDL. In addition to these characteristics, electron-microscopic analysis showed the existence of WP bodies, which are the endothelial-specific storage organelle for the regulation of vWf secretion. These results indicate MAECs are an EC line.

The differentiation of the EC lineage was assessed in a previous study [32]. Flk-1 is the early marker for endothelial progenitors and is expressed in isolated mesodermal cells that give rise to ECs and in hematopoietic cell progenitors, termed hemangioblasts. In addition, Flk-1 is expressed in various differentiation stages of ECs and is essential for EC differentiation [32–34]. Hirashima et al. [32] showed that Flk-1+ EC progenitor cells start to express VE-cadherin and CD31 and differentiate to ECs in vasculogenesis [32, 34]. Tie-2 is a receptor for both angiopoietin-1 and angiopoietin-2 and is particularly expressed in ECs [35] but also in the late stage of vascular morphogenesis [34]. Furthermore, vWf is a marker for differentiated ECs [10, 28]. We detected Flk-1 and other endothelial markers such as VE-cadherin, ICAM-2, vWf, and Tie-2 on MAECs. Therefore, these results showed that MAECs have differentiated characteristics of ECs.

Here, we investigated three functional analyses for MAECs; tube formation assay, cellular binding assay, and NO production to examine if the cell line was suitable for vascular research. The tube formation of ECs on Matrigel has been used as an in vitro angiogenesis assay [3, 4]. MAECs showed tube formation activity on Matrigel suggesting that they can be used for angiogenesis studies. MAECs also exhibited tube formation in nude mice with Matrigel, indicating that they retain the potential to organize a vascular network in vivo and that they can be used for wider applications in endothelial or vascular research. However, we have to consider that MAECs may not be the ideal model for studying angiogenesis under stressful conditions such as irradiation being imposed on the cells, because of its deficiency in p53 which plays an important role in angiogenesis [36].

Cellular binding assay is valuable for the analysis of the first step of inflammation in vitro [37, 38]. The attachment of mononuclear cells to the endothelium is essential in the initiation of atherosclerotic and inflammatory lesions, and it is well known that cell adhesion molecules play a key role in the development of inflammation and atherosclerosis [39]. TNFα-stimulated MAECs displayed cellular binding ability with WEHI-3B cells. Regarding the molecules that mediate these adhesions, various multiple adhesion molecules have been identified on activated ECs, including endothelial-leukocyte adhesion molecule-1 (E-selectin), VCAM-1, and ICAM-1. It was also demonstrated that VCAM-1 was expressed on MAECs activated by TNFα (fig. 5a). In addition, VLA-4, a ligand of VCAM-1, was expressed on WEHI-3B cells. These results demonstrated that VCAM-1 and VLA-4 contribute to the cellular binding activity of MAECs and WEHI-3B. In this manner, using MAECs, the interaction between cell adhesion molecules can be studied in detail.

Low-level NO production and a lower expression of eNOS in MAECs compared to HUVECs may result from the multiple passages of this cell line. Actually, Matsushita et al. [40] reported that eNOS activity was reduced in senescent human ECs, and shear stress induced greater eNOS expression and activity. From these results, although MAECs retained the endothelial characteristics regarding eNOS expression, the analysis of eNOS activity should be considered in various conditions, and MAECs may not be the ideal model for the study of NO and ECs.

p53 is a tumor suppressor protein that plays an important role in the cell cycle and cell growth. p53 protein deficiency causes mice to develop spontaneous tumors, and loss of p53 function results in genomic instability. Although many kinds of cell lines have been established from p53-deficient mice, in some cell lines genomic instability, accelerated growth, malignant transformation and some phenotypic changes were shown [17, 18, 41]. In this paper, our results showed that MAECs expressed vWf, whose production is often lost in transformed or malignant ECs in angiosarcomas [10, 28]. Therefore, we consider that MAECs are an established cell line which may not have obtained malignant transformation. However, further investigation will be needed regarding malignancy.

In conclusion, we propose that our EC line MAEC, which retains endothelial functions such as cellular binding activity and tube formation activity, could contribute significantly to the future study of EC biology. This cell line is freely available for the academic research community with a material transfer agreement.

Acknowledgments

This work was partially supported by grants-in-aid for scientific research from the Ministry of Education, Culture, Sports, Science and Technology of Japan. The authors gratefully thank Roger E. Morgan for helpful comments and critical reading of the manuscript, and Judith Nishino for helpful discussions during the preparation of this manuscript. The Sjögren's Syndrome Project of Keio University was supported by Kowa Co., Ltd.

References

1 Carmeliet P: Angiogenesis in health and disease. Nat Med 2003;9:653–660.
2 Jaffe EA, Nachman RL, Becker CG, Minick CR: Culture of human endothelial cells derived from umbilical veins. Identification by morphologic and immunologic criteria. J Clin Invest 1973;52:2745–2756.
3 Liu JJ, Huang TS, Cheng WF, Lu FJ: Baicalein and baicalin are potent inhibitors of angiogenesis: inhibition of endothelial cell proliferation, migration and differentiation. Int J Cancer 2003;106:559–565.
4 Chen HH, Zhou HJ, Fang X: Inhibition of human cancer cell line growth and human umbilical vein endothelial cell angiogenesis by artemisin in derivatives in vitro. Pharmacol Res 2003;48:231–236.
5 Dong QG, Bernasconi S, Lostaglio S, De Calmanovici RW, Martin-Padura I, Breviario F, Garlanda C, Ramponi S, Mantovani A, Vecchi A: A general strategy for isolation of endothelial cells from murine tissues. Characterization of two endothelial cell lines from the murine lung and subcutaneous sponge implants. Arterioscler Thromb Vasc Biol 1997;17:1599–1604.
6 Toyama-Sorimachi N, Miyake K, Miyasaka M: Activation of CD44 induces ICAM-1/LFA-1-independent, Ca^{2+}, Mg^{2+}-independent adhesion pathway in lymphocyte-endothelial cell interaction. Eur J Immunol 1993;23:439–446.
7 Kanda S, Landgren E, Ljungstrom M, Claesson-Welsh L: Fibroblast growth factor receptor 1-induced differentiation of endothelial cell line established from tsA58 large T transgenic mice. Cell Growth Differ 1996;7:383–395.
8 Lidington EA, Rao RM, Marelli-Berg FM, Jat PS, Haskard DO, Mason JC: Conditional immortalization of growth factor-responsive cardiac endothelial cells from H-2K(b)-tsA58 mice. Am J Physiol Cell Physiol 2002;282:C67–C74.
9 Harder R, Uhlig H, Kashan A, Schutt B, Duijvestijn A, Butcher EC, Thiele HG, Hamann A: Dissection of murine lymphocyte-endothelial cell interaction mechanisms by SV-40-transformed mouse endothelial cell lines: novel mechanisms mediating basal binding, and alpha 4-integrin-dependent cytokine-induced adhesion. Exp Cell Res 1991;197:259–267.
10 Masuzawa M, Fujimura T, Hamada Y, Fujita Y, Hara H, Nishiyama S, Katsuoka K, Tamauchi H, Sakurai Y: Establishment of a human hemangiosarcoma cell line (ISO-HAS). Int J Cancer 1999;81:305–308.
11 Lidington EA, Moyes DL, McCormack AM, Rose ML: A comparison of primary endothelial cells and endothelial cell lines for studies of immune interactions. Transpl Immunol 1999;7:239–246.
12 Arbiser JL, Larsson H, Claesson-Welsh L, Bai X, LaMontagne K, Weiss SW, Soker S, Flynn E, Brown LF: Overexpression of VEGF 121 in immortalized endothelial cells causes conversion to slowly growing angiosarcoma and high level expression of the VEGF receptors VEGFR-1 and VEGFR-2 in vivo. Am J Pathol 2000;156:1469–1476.
13 Tsukada T, Tomooka Y, Takai S, Ueda Y, Nishikawa S, Yagi T, Tokunaga T, Takeda N, Suda Y, Abe S, et al: Enhanced proliferative potential in culture of cells from p53-deficient mice. Oncogene 1993;8:3313–3322.
14 Nakayama T, Kanoe H, Sasaki MS, Aizawa S, Nakamura T, Toguchida J: Establishment of an osteoblast-like cell line, MMC2, from p53-deficient mice. Bone 1997;21:313–319.
15 Hasegawa S, Yamada K, Inoue H, Azuma N, Suzuki M, Matsuoka T: Establishment of pulmonary alveolar type II cell line from p53-deficient mice. Lung 2001;179:21–29.
16 Hanazono M, Nakagawa E, Aizawa S, Tomooka Y: Establishment of prostatic cell line 'Pro9ad' from a p53-deficient mouse. Prostate 1998;36:102–109.
17 Minakawa M, Sugimoto T, Aizawa S, Tomooka Y: Cerebellar cell lines established from a p53-deficient adult mouse. Brain Res 1998;813:172–176.
18 Yahanda AM, Bruner JM, Donehower LA, Morrison RS: Astrocytes derived from p53-deficient mice provide a multistep in vitro model for development of malignant gliomas. Mol Cell Biol 1995;15:4249–4259.
19 Sevignani C, Wlodarski P, Kirillova J, Mercer WE, Danielson KG, Iozzo RV, Calabretta B: Tumorigenic conversion of p53-deficient colon epithelial cells by an activated Ki-ras gene. J Clin Invest 1998;101:1572–1580.
20 Tanaka K, Sato M, Tomita Y, Ichihara A: Biochemical studies on liver functions in primary cultured hepatocytes of adult rats. I. Hormonal effects on cell viability and protein synthesis. J Biochem (Tokyo) 1978;84:937–946.
21 Weibel ER, Palade GE: New cytoplasmic components in arterial endothelia. J Cell Biol 1964;23:101–112.
22 Staunton DE, Dustin ML, Springer TA: Functional cloning of ICAM-2, a cell adhesion ligand for LFA-1 homologous to ICAM-1. Nature 1989;339:61–64.
23 Yamaguchi TP, Dumont DJ, Conlon RA, Breitman ML, Rossant J: flk-1, an flt-related receptor tyrosine kinase is an early marker for endothelial cell precursors. Development 1993;118:489–498.
24 Lynch DC, Zimmerman TS, Collins CJ, Brown M, Morin MJ, Ling EH, Livingston DM: Molecular cloning of cDNA for human von Willebrand factor: authentication by a new method. Cell 1985;41:49–56.
25 Carmeliet P, Lampugnani MG, Moons L, Breviario F, Compernolle V, Bono F, Balconi G, Spagnuolo R, Oostuyse B, Dewerchin M, Zanetti A, Angellilo A, Mattot V, Nuyens D, Lutgens E, Clotman F, de Ruiter MC, Gittenberger-de Groot A, Poelmann R, Lupu F, Herbert JM, Collen D, Dejana E: Targeted deficiency or cytosolic truncation of the VE-cadherin gene in mice impairs VEGF-mediated endothelial survival and angiogenesis. Cell 1999;98:147–157.
26 Chen CS, Toda KI, Maruguchi Y, Matsuyoshi N, Horiguchi Y, Imamura S: Establishment and characterization of a novel in vitro angiogenesis model using a microvascular endothelial cell line, F-2C, cultured in chemically defined medium. In Vitro Cell Dev Biol Anim 1997;33:796–802.
27 Sato N, Sato T, Takahashi S, Kikuchi K: Establishment of murine endothelial cell lines that develop angiosarcomas in vivo: brief demonstration of a proposed animal model for Kaposi's sarcoma. Cancer Res 1986;46:362–366.
28 Toda K, Tsujioka K, Maruguchi Y, Ishii K, Miyachi Y, Kuribayashi K, Imamura S: Establishment and characterization of a tumorigenic murine vascular endothelial cell line (F-2). Cancer Res 1990;50:5526–5530.

29 Mizuno R, Yokoyama Y, Ono N, Ikomi F, Ohhashi T: Establishment of rat lymphatic endothelial cell line. Microcirculation 2003; 10:127–131.
30 Su X, Sorenson CM, Sheibani N: Isolation and characterization of murine retinal endothelial cells. Mol Vis 2003;9:171–178.
31 Voyta JC, Via DP, Butterfield CE, Zetter BR: Identification and isolation of endothelial cells based on their increased uptake of acetylated-low density lipoprotein. J Cell Biol 1984;99:2034–2040.
32 Hirashima M, Kataoka H, Nishikawa S, Matsuyoshi N: Maturation of embryonic stem cells into endothelial cells in an in vitro model of vasculogenesis. Blood 1999;93:1253–1263.
33 Eichmann A, Corbel C, Nataf V, Vaigot P, Breant C, Le Douarin NM: Ligand-dependent development of the endothelial and hemopoietic lineages from embryonic mesodermal cells expressing vascular endothelial growth factor receptor 2. Proc Natl Acad Sci USA 1997;94:5141–5146.
34 Drake CJ, Fleming PA: Vasculogenesis in the day 6.5 to 9.5 mouse embryo. Blood 2000;95: 1671–1679.
35 Davis S, Aldrich TH, Jones PF, Acheson A, Compton DL, Jain V, Ryan TE, Bruno J, Radziejewski C, Maisonpierre PC, Yancopoulos GD: Isolation of angiopoietin-1, a ligand for the TIE2 receptor, by secretion-trap expression cloning. Cell 1996;87:1161–1169.
36 Su JD, Mayo LD, Donner DB, Durden DL: PTEN and phosphatidylinositol 3′-kinase inhibitors up-regulate p53 and block tumor-induced angiogenesis: evidence for an effect on the tumor and endothelial compartment. Cancer Res 2003;63:3585–3592.
37 Umetani M, Nakao H, Doi T, Iwasaki A, Ohtaka M, Nagoya T, Mataki C, Hamakubo T, Kodama T: A novel cell adhesion inhibitor, K-7174, reduces the endothelial VCAM-1 induction by inflammatory cytokines, acting through the regulation of GATA. Biochem Biophys Res Commun 2000;272:370–374.
38 Kaneko M, Hayashi J, Saito I, Miyasaka N: Probucol downregulates E-selectin expression on cultured human vascular endothelial cells. Arterioscler Thromb Vasc Biol 1996; 16:1047–1051.
39 Cybulsky MI, Gimbrone MA Jr: Endothelial expression of a mononuclear leukocyte adhesion molecule during atherogenesis. Science 1991;251:788–791.
40 Matsushita H, Chang E, Glassford AJ, Cooke JP, Chiu CP, Tsao PS: eNOS activity is reduced in senescent human endothelial cells: preservation by hTERT immortalization. Circ Res 2001;89:793–798.
41 Ohmi K, Masuda T, Yamaguchi H, Sakurai T, Kudo Y, Katsuki M, Nonomura Y: A novel aortic smooth muscle cell line obtained from p53 knock out mice expresses several differentiation characteristics. Biochem Biophys Res Commun 1997;238:154–158.

0022-3565/07/3202-516–524$20.00
THE JOURNAL OF PHARMACOLOGY AND EXPERIMENTAL THERAPEUTICS
Copyright © 2007 by The American Society for Pharmacology and Experimental Therapeutics
JPET 320:516–524, 2007

Vol. 320, No. 2
113092/3168709
Printed in U.S.A.

Up-Regulated PAR-2-Mediated Salivary Secretion in Mice Deficient in Muscarinic Acetylcholine Receptor Subtypes

Tatsuaki Nishiyama, Takeshi Nakamura,[1] Kumi Obara, Hiroko Inoue, Kenji Mishima, Nagisa Matsumoto, Minoru Matsui, Toshiya Manabe, Katsuhiko Mikoshiba, and Ichiro Saito

Department of Pathology, Tsurumi University School of Dental Medicine, Yokohama, Japan (T.Ni., K.O., H.I., K.Mis., I.S.); Sjogren's Syndrome Project, Shinanomachi Research Park, Keio University, Tokyo, Japan (T.Ni., I.S.); Calcium Oscillation Project, International Cooperative Research Project, Japan Science and Technology Agency, Minato-ku, Tokyo, Japan (T.Na., K.Mik.); and Divisions of Molecular Neurobiology (N.M., K.Mik.) and Neuronal Network (M.M., T.M.,), Department of Basic Medical Sciences, Institute of Medical Science, University of Tokyo, Tokyo, Japan

Received September 1, 2006; accepted October 30, 2006

ABSTRACT

Protease-activated receptor-2 (PAR-2) is expressed in the salivary glands and is expected to be a new target for the treatment of exocrine dysfunctions, such as dry mouth; however, the salivary secretory mechanism mediated by PAR-2 remains to be elucidated. Therefore, mechanism of the PAR-2-mediated salivary secretion was investigated in this study. We found that a PAR-2 agonist peptide, SLIGRL-OH, induced salivary flow in vivo and dose-dependent increase in $[Ca^{2+}]_i$ submandibular gland (SMG) acinar cells in wild-type (WT) mice and mice lacking M_3 or both M_1 and M_3 muscarinic acetylcholine receptors (mAChRs), whereas secretions in PAR-2 knockout (PAR-2KO) mice were completely abolished. The saliva composition secreted by SLIGRL-OH was similar to that secreted by mAChR stimulation. Ca^{2+} imaging in WT acinar cells and β-galactosidase staining in PAR-2KO mice, in which the β-galactosidase gene (*LacZ*) was incorporated into the disrupted gene, revealed a nonubiquitous, sporadic distribution of PAR-2 in the SMG. Furthermore, compared with the secretion in WT mice, PAR-2-mediated salivary secretion and Ca^{2+} response were enhanced in mice lacking M_3 or both M_1 and M_3 mAChRs, in which mAChR-stimulated secretion and Ca^{2+} response in acinar cells were severely impaired. Although the mechanism underlying the enhanced PAR-2-mediated salivary secretion in M_3-deficient mice is not clear, the result suggests the presence of some compensatory mechanism involving PAR-2 in the salivary glands deficient in cholinergic activation. These results indicate that PAR-2 present in the salivary glands mediates Ca^{2+}-dependent fluid secretion, demonstrating potential usefulness of PAR-2 as a target for dry mouth treatment.

PAR-2, isolated and cloned from a mouse genomic library (Nystedt et al., 1994), belongs to a large superfamily of G protein-coupled receptors. PAR-2 is activated by proteolytic unmasking of the N-terminal extracellular tethered ligand that binds to the extracellular loop 2 of the receptor itself (Lerner et al., 1996; Al-Ani et al., 1999; Al-Ani and Hollenberg, 2003). Serine proteases, including trypsin and tryptase, are endogenous activators of PAR-2, and the cleavage mediated by these proteases generated a distinct N-terminal tethered ligand sequence (SLIGRL and SLIGKV for murine and human PAR-2, respectively) (Nystedt et al., 1994; Kawabata and Kuroda, 2000; Macfarlane et al., 2001). Synthetic peptides based on the receptor-activating sequence of the tethered ligand (SLIGRL and SLIGKV) are also capable of activating PAR-2 by direct binding to the receptor (Kawabata et al., 2000a,b, 2001, 2002b; Oshiro et al., 2002). Since its cloning, the expression and functional role of PAR-2 have been elucidated in various tissues (Kawabata et al., 2000a, 2001, 2002b; Macfarlane et al., 2001). Various physiological/pathophysiological roles of PAR-2 have been identified. PAR-2 seems to play a role in inflammation (Kawagoe et al., 2002), and it has also been shown that PAR-2 present in sensory neurons causes pain sensation and hyperalgesia (Kawabata et al., 2002a). Recent studies regarding the effect of PAR-2

The Sjogren's Syndrome Project of Keio University was supported by Kowa Co., Ltd. This study was funded by Pharmacia; Detrol LA Research Grant Program was supported by Pfizer; The Industrial Technology Research Grant Program 02A09001a was supported by The New Energy and Industrial Technology Development Organization of Japan, and Grant-in-aid for Scientific Research on Priority Areas 16067101 was supported by The Ministry of Education, Culture, Sports, Science and Technology.

[1] Deceased in July 23, 2006.

Article, publication date, and citation information can be found at http://jpet.aspetjournals.org.
doi:10.1124/jpet.106.113092.

ABBREVIATIONS: PAR-2, protease-activated receptor-2; SMG, submandibular gland; WT, wild type; mAChRs, muscarinic acetylcholine receptors; PAR-2KO, PAR-2 knockout; KO, knockout; SS, Sjogren's syndrome; TG, transgenic mice; HE, hematoxylin and eosin; BSS, balanced salt solution; BSA, bovine serum albumin; CCh, carbachol.

activation on exocrine tissues have reported that agonist peptides for PAR-2 induce exocrine secretion in the salivary gland, the lacrimal gland, the gastrointestinal tract, and the pancreas (Kawabata et al., 2000a, 2001, 2002b). The results demonstrate a novel secretory mechanism in these exocrine tissues and, thus, suggest that PAR-2 is a possible molecular target for the treatment of exocrine gland dysfunctions.

Xerostomia is a condition caused by lack of saliva in the oral cavity, and the primary causes are medications, Sjogren's syndrome (SS), irradiation of the head and neck, and aging (Bivona, 1998). Living with dry mouth conditions can be a harrowing experience for the sufferer; therefore, stimulating salivary output is a clinical goal for the treatment of xerostomia. From a molecular basis, salivary secretion is mainly regulated by M_3-mediated cholinergic stimulation in the salivary gland cells (Maeda et al., 1988; Nakamura et al., 2004).

In fact, pilocarpine and cevimeline, which both stimulate mAChRs, have been clinically used. However, some SS patients have autoantibodies against the mAChR (Bacman et al., 2001; Nagaraju et al., 2001). Furthermore IgG from SS patients and anti-M_3 antibody reduced Ca^{2+} signaling in both human and mouse submandibular acinar cells (Bacman et al., 2001; Nagaraju et al., 2001; Dawson et al., 2006). In addition, side effects, such as sweating, flushing, and urinary frequency, are common in mAChR stimulants (Wiseman and Faulds, 1995). Furthermore, use of pilocarpine is contraindicated in patients with uncontrolled asthma, narrow-angle glaucoma, or acute iritis, and caution is advised with use in patients with cardiovascular disease (Wiseman and Faulds, 1995). Therefore, development of other types of drugs to stimulate salivary flow with different mechanisms would be of clinical relevance in terms of the proper choice of drugs suitable for individual patients.

As mentioned above, recent studies have shown that the PAR-2 agonist mediated the exocrine secretions, including secretion of mucus in rat stomach (Kawabata et al., 2001), *N*-acetylneuraminic acid in rat sublingual gland (Kawabata et al., 2000a), and pancreatic and salivary amylase in rats (Kawabata et al., 2002b). Salivary fluid secretion, also induced by PAR-2 activation in mice and rats, was not inhibited by antagonists for mAChR, α-adrenergic, or β-adrenergic receptors (Kawabata et al., 2000b), indicating that the PAR-2 agonist does not stimulate these secretion-related receptors known to date in the salivary glands. Investigation of PAR-2 expression by reverse transcription-polymerase chain reaction or immunohistochemistry showed that it was expressed in rat pancreas, submandibular gland, parotid gland, and sublingual gland (Kawabata et al., 2000a,b, 2002b). However, it has not been investigated whether salivary fluid secretion can be induced by direct stimulation of PAR-2 present in the salivary glands. Although PAR-2-mediated generation of Ca^{2+} signaling was reported in some cells (Oshiro et al., 2002; Kawabata et al., 2004b), no examination has been conducted in salivary gland cells.

The purpose of the present study is to characterize the salivary secretion stimulated by PAR-2 and to explore the $[Ca^{2+}]_i$ increase using WT, PAR-2KO and mAChRKO mice (M_1KO, M_3KO, and M_1/M_3KO mice). Specifically, the following points were investigated in these mice: 1) amylase and protein concentrations in PAR-2-induced saliva; 2) the amount and time course of PAR-2-induced salivary secretion; 3) generation of intracellular Ca^{2+} signaling in response to PAR-2 activation in salivary gland acinar cells, and 4) distribution of PAR-2 in the salivary glands. The results indicate that PAR-2 mediates Ca^{2+}-dependent fluid secretion in the salivary glands and is potentially useful as a molecular target for dry mouth treatment.

Materials and Methods

All experiment procedures were approved by the animal welfare committees of Tsurumi University and the University of Tokyo (Tokyo, Japan).

Mutant Mice. Generation and characterization of mAChRKO mice (M_1KO, M_3KO, and M_1/M_3KO mice) have been described previously (Matsui et al., 2000; Ohno-Shosaku et al., 2003), and the mice used were maintained by backcrossing for at least 7 (M_1KO), 10 (M_3KO), or 3 (M_1/M_3KO) generations with C57BL/6J mice (CLEA Japan, Tokyo, Japan) that were used as WT mice. Generation and characterization of PAR-2KO mice have been described previously (Ferrell et al., 2003). A bacterial *LacZ* was inserted downstream of the *PAR-2* promoter. PAR-2KO mice were maintained by backcrossing for eight generations with C57BL/6J mice (CLEA Japan) and then supplied by Kowa Co. Ltd. (Tokyo, Japan). β-galactosidase transgenic (TG) mice were purchased from the Jackson Laboratory (Bar Harbor, ME). This mutant was made by a retroviral insertion into embryonic stem cells. *LacZ* was under an unknown endogenous promoter and expressed in most tissues of adult mouse (strain name: B6.129S7-*Gt(ROSA)26Sor/J*, stock number: 001292). The lights in the animal room were turned on between 7:00 AM and 7:00 PM. The mice were fed standard dry pellets, CA-1 (CLEA Japan), and water ad libitum. To improve the growth of M_3KO and M_1/M_3KO mice, hydrated paste food was prepared by mixing the powder form of CA-1 (CLEA Japan) with twice the weight of sterilized tap water and was given to the litters from the age of 2 weeks until the age of 8 weeks.

Histologic Analysis. WT (n = 7), M_1KO (n = 18), M_3KO (n = 6), M_1/M_3KO (n = 6), and PAR-2KO (n = 24) mice were anesthetized with a mixture of 36 mg/kg ketamine (Sigma, St. Louis, MO) and 16 mg/kg xylazine (Sigma) and sacrificed. SMGs were removed and fixed with 4% phosphate-buffered formaldehyde and embedded in paraffin. The sections (4 μm) were prepared and stained with hematoxylin and eosin (HE) for histologic examination.

SMGs freshly isolated from PAR-2KO mice, anesthetized and sacrificed as described above, were embedded in Optimal Cutting temperature compound (OCT; Sakura Finetechnical, Tokyo, Japan) and frozen in liquid nitrogen. Cryostat sections (5 μm) were made, and the sections were stained for β-galactosidase activity. The sections were then fixed in phosphate-buffered saline (pH 7.2) containing 0.25% glutaraldehyde for 10 min at 4°C and stained in 5 mM $K_4Fe(CN)_6 \cdot 3H_2O$, 5 mM $K_3Fe(CN)_6$, 0.2 mM $MgCl_2$, and 1 mg of 5-bromo-4-chloro-3-indolyl-β-D-galactopyranoside (X-gal)/ml in phosphate-buffered saline (pH 7.2) overnight at 37°C. They were then rinsed in phosphate-buffered saline (pH 7.2) and stained with hematoxylin at room temperature for better visualization of the staining. The sections were examined by light microscopy, and pictures were taken with original magnification of 40× objective lens.

Measurement of Salivary Secretion. Salivary secretion was measured in vivo in 10 to 15-week-old male WT (n = 7), M_1KO (n = 5), M_3KO (n = 5), M_1/M_3KO (n = 5), and PAR-2KO (n = 5) mice. The mice were anesthetized i.p. with a mixture of 36 mg/kg ketamine and 16 mg/kg xylazine and then injected with either 18 mg/kg SLIGRL-OH (Peptide Institute Inc., Osaka, Japan) i.v., 5 mg/kg pilocarpine-HCl (sanpilo 1%; Santen Pharmaceutical Co. Ltd., Osaka, Japan) i.p., or 0.5 mg/kg isoproterenol (Sigma) i.p. The saliva secreted into the oral cavity during each 1-min period following an injection of either of the above stimulants was carefully collected using capillaries for 15 min after the injection (ringcaps; Hirschmann Laborgerate GmbH & Co. KG, Eberstadt, Germany).

Analysis of Amylase Activity and Total Protein Concentration in Secreted Saliva. The secreted saliva was collected for a period of 15 min after administration of the stimulant as described above and was subjected to amylase activity assay. The amount of amylase in the collected saliva was measured by the colorimetric method using Amylase Test Wako (Wako Pure Chemicals, Osaka, Japan). Total protein concentration in the secreted saliva was determined using bicinchoninic acid protein assay kit (Pierce, Rockford, IL).

SMG Cell Preparation. Three-to-four-month-old mice were used for the experiments. Each mouse was anesthetized with a mixture of 36 mg/kg ketamine and 16 mg/kg xylazine and sacrificed. The bilateral SMGs were immediately removed and placed in ice-cold balanced salt solution (BSS) containing 115 mM NaCl, 5.4 mM KCl, 2 mM Ca^{2+}, 1 mM Mg^{2+}, 20 mM HEPES, and 10 mM glucose, pH 7.4, supplemented with 1.25% bovine serum albumin (BSS-BSA), and rapidly minced. The material was then digested for 20 min at 37°C with 2 mg/ml collagenase type-2 (Worthington, Malvern, PA) in BSS-BSA. The suspension was gently passed through a pipette 20 times every 10 min. After digestion, the preparation was centrifuged at 70 g for 2 min and then the pellet was resuspended in 10 ml of BSS-BSA, rinsed twice, and filtered through a 100-μm nylon mesh (Cell Strainer 100 μm; BD Biosciences, Bedford, MA) to generate a batch of SMG cells.

Measurement of the Intracellular Ca^{2+} Concentration. The isolated SMG cell preparation was loaded with fura-2 by incubation for 1 h at room temperature with 3 μM fura-2/acetoxymethyl ester (Dojindo, Kumamoto, Japan) suspended in BSS-BSA, rinsed twice, resuspended in 4 ml of BSS-BSA, and stored at 4°C. Ratiometric measurement of fura-2 fluorescence was made using a spectrofluorometer (CAF-110; Jasco, Tokyo, Japan). A 500-μl sample of fura-2-loaded SMG cells was transferred to a glass cuvette and alternately illuminated with 340- and 380-nm excitation light; the resultant fluorescence (510 ± 10 nm) was collected at 25 Hz. SLIGRL-OH (10, 30, 100, and 300 μM) and 30 μM carbachol (CCh) were added directly to the cell suspension during fluorescence recordings. At the end of each experiment, the R_{max} was determined by adding 0.2% Triton X-100 to the cuvette, and then the R_{min} was determined by adding 10 mM EGTA; these values were then used to calculate the $[Ca^{2+}]_i$ using Grynkiewicz's equation (Grynkiewicz et al., 1985). The fluorescence intensities excited by 340- and 380-nm wavelength light (F_{340} and F_{380}, respectively) and the ratios (F_{340}/F_{380}) were digitized with 12-bit resolution and stored and displayed in a personal computer using the MacLab4/s system (AD Instruments-Japan, Tokyo, Japan).

For two-dimensional measurement of $[Ca^{2+}]_i$ changes, a small aliquot (20–50 μl) of fura-2-loaded SMG cell suspension was dispersed on the Cell-Tak coated glass (BD Biosciences, Bedford, MA) that formed the bottom of the recording chamber and then mounted on the stage of an inverted fluorescence microscope (IX70; Olympus, Tokyo, Japan) and perfused with BSS at a rate of 2 ml/min at room temperature. Excitation of fura-2 was made every 5 s by an alternate illumination of 340- and 380-nm light, and the resultant fluorescence (510–550 nm; F_{340} and F_{380}) was collected using an objective lens (UPlanApo 20x/340; Olympus) and silicon-intensified target camera (Hamamatsu Photonics, Hamamatsu, Japan), processed to obtain pseudo-colored images of F_{340}/F_{380}, and stored in a personal computer using the software ARGUS50/CA (Hamamatsu Photonics).

Chemicals. PAR-2 agonist peptide SLIGRL-OH and 2-furoylated-LIGRL-NH_2 were prepared by standard solid-phase synthesis procedure. The concentration, purity, and composition of the peptides were determined by high-performance liquid chromatography, mass spectrometry, and quantitative amino acid analysis. Pilocarpine-HCl was purchased as sanpilo 1% from Santen Pharmaceutical Co. Ltd. Isoproterenol and CCh were purchased from Sigma.

Statistics. Data were calculated as the mean ± S.E.M. in the text and figures, and p values were determined using Dunnett's multiple comparisons (Figs. 2 and 4) or Scheffe's test (Fig. 3). $p < 0.05$ was considered significant.

Results

Histologic Analysis. The SMGs were subjected to histologic analysis by HE staining to study whether any morphological changes were caused by deficiency in PAR-2KO, M_1KO, M_3KO, or both M_1 and M_3KO mice. As reported previously (Matsui et al., 2000), M_3KO mice showed normal histology. Furthermore, no histologic abnormalities were found in the M_1/M_3KO or PAR-2KO mice (Fig. 1). In this context, deficiency of M_1, M_3, and PAR-2 are unlikely to be involved in the morphogenesis of the SMG.

Measurement of Saliva. Although it is reported that systemic administration of PAR-2 agonists induced salivary secretion in previous investigations (Kawabata et al., 2000b, 2004a), PAR-2 activation in the salivary gland has not been shown yet. Therefore, the fact that M_3 plays a central role in

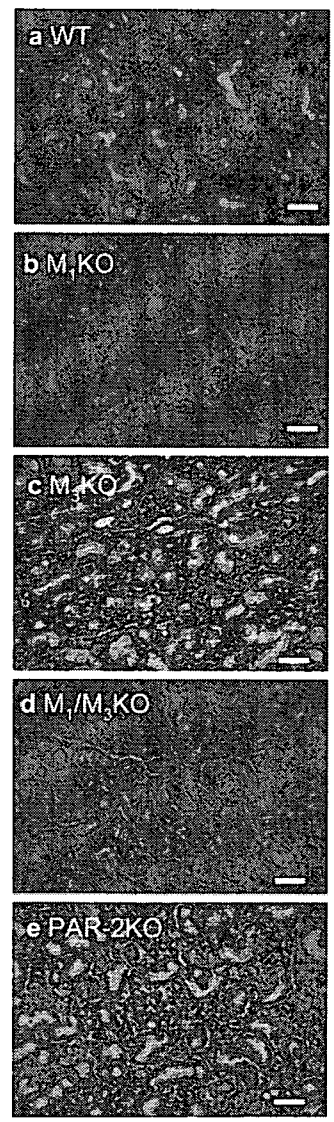

Fig. 1. Histologic analysis of the SMGs was taken from WT (a), M_1KO (b), M_3KO (c), M_1/M_3KO (d), and PAR-2KO (e) mice. All pictures showing HE staining of the SMG cells were taken with original magnification of 10 × 20 lenses. Scale bar is 20 μm.

the control of salivary secretion (Nakamura et al., 2004) raises a possibility that systemic administration of SLIGRL-OH may induce cholinergic activation via PAR-2, which is expressed ubiquitously (Macfarlane et al., 2001). To examine this possibility, salivary secretion was measured in vivo in WT, PAR-2KO, and mAChRKO mice (M_1KO, M_3KO, and M_1/M_3KO), among which M_3 and M_1/M_3 KO mice had impairment of cholinergically stimulated Ca^{2+} signaling and salivary secretion. Figure 2, a through c, shows the saliva output for each 1-min period after stimulant injection, and Fig. 2, d through f, shows the cumulative amounts of saliva secreted in 15 min. When 5 mg/kg pilocarpine was injected i.p. into anesthetized mice, the cumulative amount of saliva secreted in 15 min was 4.2 ± 1.3 μl/g in M_3KO and 0 μl/g in M_1/M_3KO mice, whereas considerable salivary secretion was induced in WT (13.3 ± 1.0 μl/g), M_1KO (13.2 ± 0.6 μl/g), and PAR-2KO (13.3 ± 0.7 μl/g) mice.

Although SLIGRL-OH evoked salivary secretion equally in WT (1.6 ± 0.2 μl/g) and M_1KO mice (2.1 ± 0.3 μl/g), no saliva was detected in the PAR-2KO mice, as reported previously (Kawabata et al., 2004a). However, it was notable that SLIGRL-OH-induced salivary secretion relative to body weight was significantly increased in M_3KO (3.0 ± 0.3 μl/g) and M_1/M_3KO mice (3.4 ± 0.1 μl/g) compared with WT mice (Fig. 2e, $p < 0.001$). The body weights of mice used were 25.0 ± 0.7 g (WT), 22.8 ± 0.6 g (M_1KO), 23.0 ± 1.6 g (M_3KO), 22.3 ± 1.2 g (M_1/M_3KO), and 23.8 ± 0.8 g (PAR-2KO). Statistical difference was not detected in the body weights. PAR-2-activated salivary secretion lasted only for 5 min after administration (Fig. 2b), and the amount of secreted saliva by pilocarpine was eight times larger than that by SLIGRL-OH. The difference in route of administration (i.p. versus i.v.) and rapid degradation of SLIGRL-OH (Hollenberg et al., 1993; Kawabata et al., 2000b) may explain the transient time course of PAR-2-mediated salivary secretion. Actually, SLIGRL-OH induced salivary secretion only by i.v. administration without amastatin. Since Kawabata et al. (2004a) reported 2-furoylated-LIGRL-NH_2 as potent and metabolically

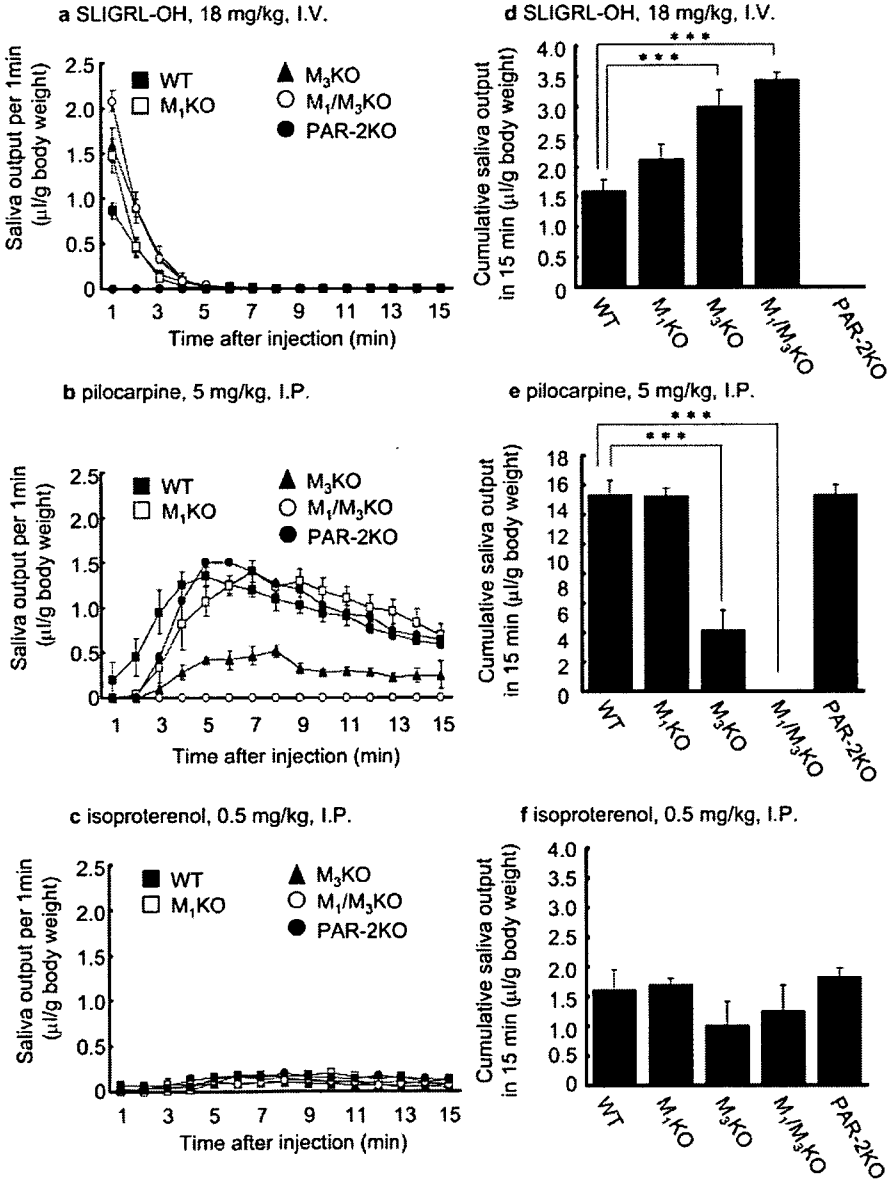

Fig. 2. Salivary secretion in WT, M_1KO, M_3KO, M_1/M_3KO, and PAR-2KO mice. a to c, saliva output for each 1-min period after injection is represented by the symbols and lines in the left panels. d to f, the cumulative amount in 15 min in the right panels. a and d, salivary secretion in response to 18 mg/kg SLIGRL-OH i.v.. b and e, 5 mg/kg pilocarpine i.p. c and f, 0.5 mg/kg isoproterenol i.p. in WT ($n = 7$), M_1KO ($n = 5$), M_3KO ($n = 5$), M_1/M_3KO ($n = 5$), and PAR-2KO ($n = 5$) mice. d, significantly larger values in M_3KO and M_1/M_3KO mice are depicted by asterisks (***, $p < 0.001$ compared with WT mice). e, significantly smaller values in M_3KO and M_1/M_3KO mice are depicted by asterisks (***, $p < 0.001$ compared with WT mice).

stable modified agonists, 2-furoylated-LIGRL-NH_2 was used to analyze the effect of administration route. 2-Furoylated-LIGRL-NH_2 (0.6 mg/kg) induced salivary secretion in WT mice (3.6 ± 0.3 μl/g i.v., 5.9 ± 0.1 μl/g i.p., 6.0 ± 0.5 μl/g s.c., or 1.7 ± 0.5 μl/g p.o.). These results demonstrated that potent and metabolically stable agonists induce larger salivary secretion and that 2-furoylated-LIGRL-NH_2 may be degraded by oral administration.

Isoproterenol-induced salivary secretions were much less than pilocarpine-induced secretions: 1.6 ± 0.3 μl/g in WT, 1.7 ± 0.1 μl/g in M_1KO, 1.0 ± 0.4 μl/g in M_3KO, 1.3 ± 0.4 μl/g in M_1/M_3KO, and 1.8 ± 0.2 μl/g in PAR-2KO mice, which are consistent with the fact that β-adrenergic, sympathetic stimulation evokes water secretion only slightly but mainly induces protein secretion after production of cyclic adenosine monophosphate (Slomiany et al., 1992).

The salivary response of mAChRKO mice caused by pilocarpine or isoproterenol administration concurs with a previous report (Nakamura et al., 2004). The results that the activation of PAR-2 caused salivary secretion in M_1/M_3KO mice strongly suggest that the secretion was not mediated by the activation of the cholinergic stimulation but caused by a direct activation of PAR-2.

Comparison of Saliva Composition Secreted in Response to SLIGRL-OH, Pilocarpine, and Isoproterenol. To characterize the secretory pathway activated by PAR-2, composition of the saliva secreted in response to SLIGRL-OH was compared with saliva secreted in response to pilocarpine or isoproterenol in WT mice. The activities of amylase in concentration (1684 ± 220 U/μl; Fig. 3a, $n = 14$) in the saliva secreted in response to SLIGRL-OH were closer to those secreted in response to pilocarpine (2443 ± 220 U/μl, $n = 15$) than those in the saliva secreted in response to isoproterenol, which showed much higher activity (17137 ± 887 U/μl, $n = 11$, $p < 0.001$, comparing isoproterenol to pilocarpine or SLIGRL-OH). In the point of total amylase activity secreted in 15 min, the activities of amylase (1697 ± 300 U/15 min g body weight) in saliva secreted in response to SLIGRL-OH were lower than those in response to pilocarpine (40813 ± 6070 U/15 min g body weight, $p < 0.001$, comparing pilocarpine to SLIGRL-OH) or isoproterenol (23876 ± 5180 U/15 min g body weight, $p < 0.05$, comparing isoproterenol to SLIGRL-OH). This high amylase activity in the saliva secreted in response to pilocarpine is dependent on the larger volume of saliva induced by pilocarpine.

There was no statistically significant difference between protein concentration in the saliva secreted in response to SLIGRL-OH (0.98 ± 0.1 mg/ml; Fig. 3b $n = 17$) and that in response to pilocarpine (0.94 ± 0.2 mg/ml, $n = 10$). The saliva secreted in response to isoproterenol demonstrated significantly high protein concentration (26.6 ± 2.5 mg/ml, $n = 17$, $p < 0.01$, comparing isoproterenol to pilocarpine or SLIGRL-OH). Regarding the mass of protein secretion in 15 min, total protein in saliva secreted in response to isoproterenol (47.0 ± 12.2 μg/15 min g body weight, $p < 0.05$ or $p < 0.01$, comparing isoproterenol to pilocarpine or SLIGRL-OH) was much higher than that in response to pilocarpine (18.4 ± 3.9 μg/15 min g body weight) or SLIGRL-OH (3.3 ± 1.1 μg/15 min g body weight). In summary, composition of SLIGRL-OH-induced saliva was similar to that of pilocarpine-induced saliva rather than that of β-adrenergic stimulation (isoproterenol)-induced saliva, which contains abundant proteins (Slomiany et al., 1992). However, the ability of SLIGRL-OH to induce salivary secretion was lower than that of pilocarpine as shown in the total amylase activity.

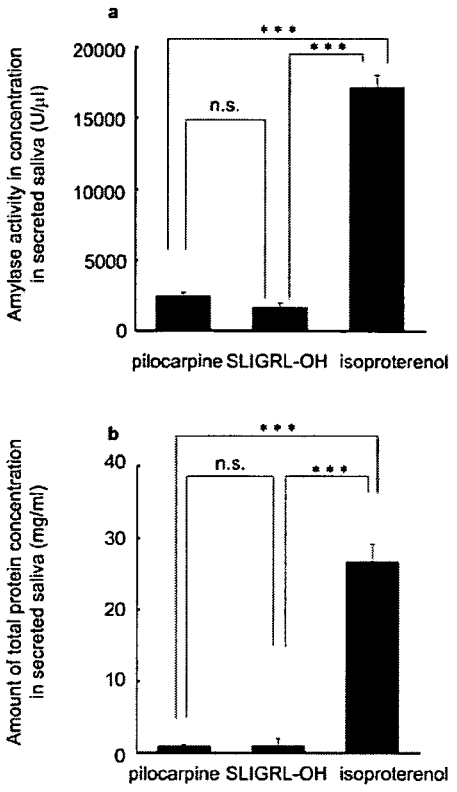

Fig. 3. Amylase activity in concentration and total protein concentration in secreted saliva. a, amylase activity in concentration. b, the total protein concentration in secreted saliva by pilocarpine ($n = 15$ for amylase activity in concentration, $n = 10$ for protein concentration), SLIGRL-OH ($n = 14$ for amylase activity in concentration, $n = 17$ for protein concentration), and isoproterenol ($n = 11$ for amylase activity in concentration, $n = 17$ for protein concentration). Statistical significance is depicted by asterisks (***, $p < 0.001$).

Increase in the Intracellular Ca^{2+} Concentration. PAR-2-mediated Ca^{2+} signaling in some cells was demonstrated similar to other G protein-coupled receptors (Oshiro et al., 2002; Kawabata et al., 2004a). As shown above, activation of PAR-2, similarly to mAChRs, seems to lead to fluid secretion in the salivary glands but not to significant amylase secretion. Taken together with the fact that the mAChR-mediated secretion is Ca^{2+}-dependent (Nakamura et al., 2004), we considered that PAR-2-induced salivary secretion is also mediated by Ca^{2+}-dependent mechanism. Therefore, we examined the Ca^{2+} signaling induced by cholinergic stimulation and SLIGRL-OH in the SMG cells. The $[Ca^{2+}]_i$ in enzymatically dispersed SMG cells from WT, M_3KO, M_1/M_3KO, and PAR-2KO mice was measured ratiometrically using fura-2. Figure 4, a through d, shows typical $[Ca^{2+}]_i$ increases in the SMG cells isolated from each specific genotype mouse in response to stimulation with SLIGRL-OH at 10, 30, 100, and 300 μM, and CCh, a nonselective cholinergic agonist, at 30 μM. Figure 4, e and f, shows the summarized results. CCh-induced $[Ca^{2+}]_i$ increases were similar to those reported previously (Nakamura et al., 2004); CCh (30 μM)-induced $[Ca^{2+}]_i$ increases were significantly reduced (8.3% WT mice, $p < 0.001$) in M_3KO mice (32.4 ± 5.1 nM) compared with WT mice (325.4 ± 14.0 nM), and no $[Ca^{2+}]_i$ increase was

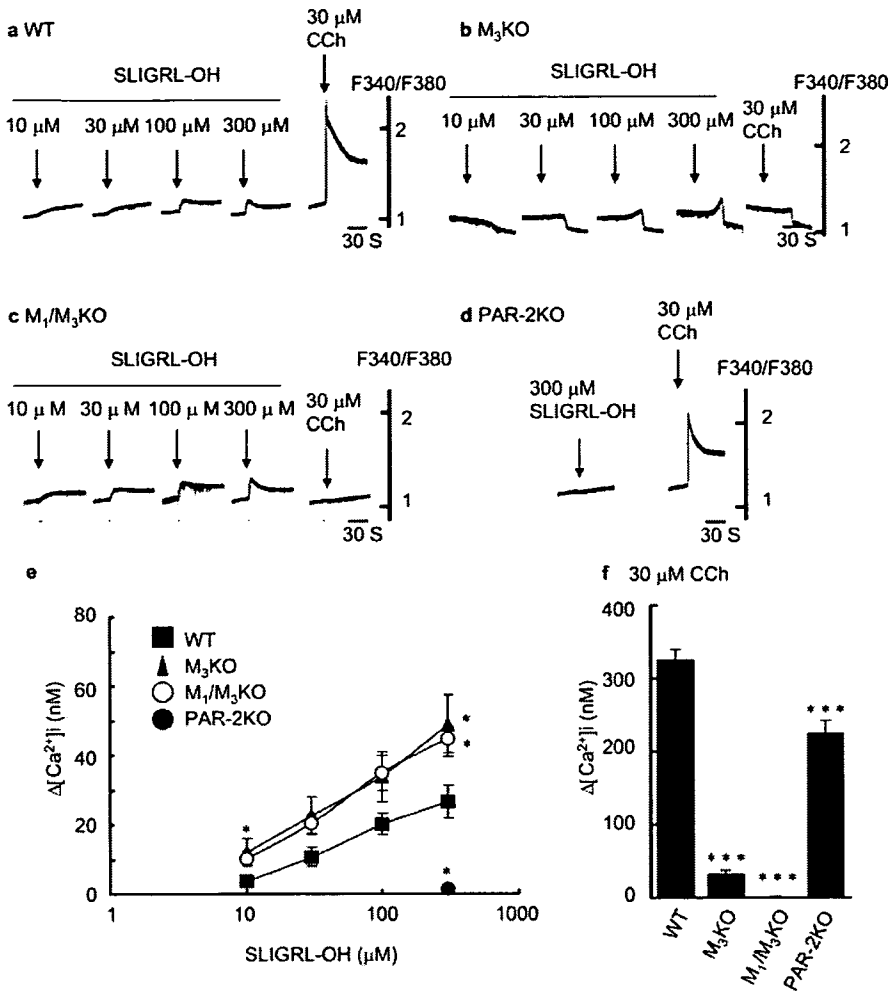

Fig. 4. CCh and SLIGRL-OH-induced $[Ca^{2+}]_i$ increase in WT, M_3KO, M_1/M_3KO, and PAR-2KO SMG cells. a through d, typical responses in individual SMG cell suspensions. SLIGRL-OH or CCh was applied to the SMG cells at the time point indicated by the arrows. The results shown are representative of six experiments. e and f, summarized peak $[Ca^{2+}]_i$ increases induced by SLIGRL-OH or CCh in WT, M_3KO, M_1/M_3KO, and PAR-2KO SMG cells (n = 9 for WT, n = 6 for M_3KO, n = 9 for M_1/M_3KO, n = 3 PAR-2KO). The $[Ca^{2+}]_i$ was calculated using the equation described by Grynkiewicz et al. (1985). Statistical significance is depicted by asterisks (*, $p < 0.05$ and ***, $p < 0.001$ compared to WT mice).

seen in M_1/M_3KO mice (1.0 ± 1.0 nM, $p < 0.001$). In PAR-2KO mice, CCh induced a large $[Ca^{2+}]_i$ increase (224.6 ± 17.9 nM); however, the magnitude of the $[Ca^{2+}]_i$ increase was significantly smaller than that in WT mice ($p < 0.001$). So far, we do not know the clear reason for this smaller response in PAR-2 KO SMG cells.

SLIGRL-OH elicited $[Ca^{2+}]_i$ increase in a dose-dependent manner at concentrations of 10 to 300 μM in the SMG cells from M_3KO, M_1/M_3KO and WT mice, whereas SLIGRL-OH did not induce any $[Ca^{2+}]_i$ changes in the SMG cells from PAR-2KO mice. These results show that PAR-2 present in the SMG is responsible for the $[Ca^{2+}]_i$ increase in response to SLIGRL-OH, regardless of the presence of mAChRs. These results are consistent with the in vivo salivary secretion (Fig. 2). SLIGRL-OH induced significantly larger $[Ca^{2+}]_i$ increases in M_3KO (48.6 ± 8.9 nM) and M_1/M_3KO (44.6 ± 3.9 nM) SMG cells, compared with those in WT (26.4 ± 4.7 nM) SMG cells at a concentration of 300 μM (statistical significance determined using Dunnett's multiple comparisons, $p < 0.05$, respectively), which may explain the enhanced salivary secretion by SLIGRL-OH in M_3KO and M_1/M_3KO mice (Fig. 2).

PAR-2 Distribution in the SMG. We next monitored $[Ca^{2+}]_i$ changes in the SMG acinar cells using a two-dimensional fluorescent digital videomicroscopy technique. Figure 5, a and b, shows the $[Ca^{2+}]_i$ changes in response to 300 μM SLIGRL-OH and 30 μM CCh in individual acinar cell clusters, each containing a few tens of acinar cells prepared from WT (Fig. 5a) or PAR-2KO (Fig. 5b) mice. The two-dimensional analysis in the WT SMG revealed that stimulation with SLIGRL-OH caused $[Ca^{2+}]_i$ increase in a punctate fashion in single acinar clusters. Moderate $[Ca^{2+}]_i$ increase was induced in limited regions of the clusters (e.g., regions of interest 1–3 in Fig. 5a) in response to 300 μM SLIGRL-OH, whereas little or very slight $[Ca^{2+}]_i$ increase was seen in some regions (e.g., regions of interest 4 and 5). SLIGRL-OH-induced $[Ca^{2+}]_i$ increase was, overall, smaller in magnitude than CCh-induced $[Ca^{2+}]_i$ increase in the WT SMG acinar cells and was not seen at all in PAR-2KO SMG acinar cells (Fig. 5b). By contrast, CCh at 30 μM induced a large $[Ca^{2+}]_i$ increase in almost the entire region of the acinar clusters in both WT and PAR-2KO mice. These results suggest that the expression level of PAR-2 is not equalized among the acinar cells in the SMG but that a certain population of acinar cells expresses PAR-2 enough to cause $[Ca^{2+}]_i$ signaling on activation.

The targeted locus of PAR-2KO mice used in this study harbors an insertion of the bacterial β-galactosidase reporter, *LacZ*, under independent translational control; detection of enzyme activity in cryosections allows us to anticipate the pattern and level of transcription of the endogenous PAR-2 gene in tissues. Using this PAR-2KO mouse line,

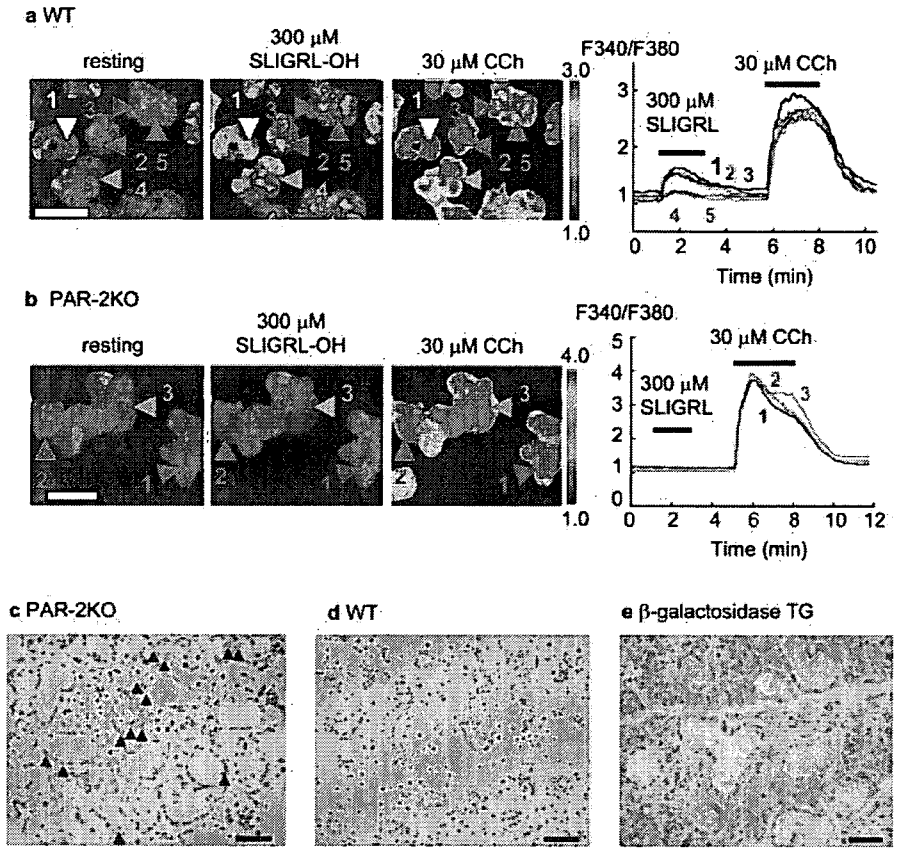

Fig. 5. PAR-2 distribution shown by Ca^{2+} imaging and β-galactosidase staining in the SMG. Pseudo-colored F_{340}/F_{380} images of WT (a) or PAR-2KO SMG (b) acinar clusters, each containing a few tens of acinar cells under resting, SLIGRL-OH-, and CCh-stimulated conditions, are shown in the left three panels, respectively. Scale bars indicate 100 μm. The right panel demonstrates temporal changes in F_{340}/F_{380} in the regions depicted by the numbered arrowheads in the pseudo-color images. The results shown represent at least eight separate measurements for each genotype. Double staining by β-galactosidase and hematoxylin for the nucleus in the SMGs of PAR-2KO (c), WT (d), and β-galactosidase (e) TG mice. Scale bars indicate 40 μm.

PAR-2 distribution in the SMG was examined by β-galactosidase staining (Rose et al., 2001). β-Galactosidase TG mice were used as positive controls under the same experimental condition to indicate the sensitivity of this staining in the PAR-2KO SMG. In contrast to the ubiquitous positive staining pattern for β-galactosidase in the positive control SMG, a scattered positive staining pattern was obtained in the PAR-2KO SMG, indicating that PAR-2 is not ubiquitously expressed in the SMG (Fig. 5c). This is consistent with the result shown by Ca^{2+} imaging in WT mice (Fig. 5a).

Discussion

Our purpose in this study is to characterize PAR-2 as a novel therapeutic target for deficiency of salivary secretion, such as dry mouth; therefore, we investigated the involvement of Ca^{2+} signaling in PAR-2-mediated salivary secretion. As described in the Introduction, PAR-2 was shown to induce salivary secretion (Kawabata et al., 2000a,b, 2002b), and there are two possibilities for the secretion mechanism. The first possibility is that PAR-2 in the SMG directly induces salivary secretion, and the second is that PAR-2 causes autonomic nervous system activation, which secondarily induces salivary secretion. In the rat gastrointestinal tract, SLIGRL-NH_2 induced gastric mucus secretion that was mediated by calcitonin gene-related peptide receptor and neurokinin-2 receptor activation (Kawabata et al., 2001).

Therefore, in our present study, we used mAChRKO (M_1KO, M_3KO, and M_1/M_3KO) mice to investigate the involvement of the parasympathetic nervous system in PAR-2-mediated salivary secretion. The results in Fig. 2 showed that SLIGRL-OH administration induced salivary secretion in mAChRKO mice, including M_1/M_3KO mice, in which no salivary secretion was induced by parasympathetic activation (Nakamura et al., 2004), and this is further confirmed by the observation that IP_3 production is required for the exocrine secretion (Futatsugi et al., 2005). Our result is consistent with the anecdotal report that atropine (7.2 μmol/kg) did not attenuate salivary secretion evoked by PAR-2-activating peptide (Kawabata et al., 2000b). In addition, SLIGRL-OH administration did not induce any salivary secretion in PAR-2KO mice, which is also consistent with a previous report (Kawabata et al., 2004a). Because there are some nonacetylcholine substances that activate the parasympathetic nervous system, such as substance P, calcitonin-gene-related peptide, and vasoactive intestinal peptide (Ekstrom, 1987), these nonacetylcholine substances might induce some salivary secretion, even in mAChRKO mice. However, they are not major salivary secretion activators (Ekstrom, 1987), and the PAR-2-induced salivary secretion was significant. Therefore, we consider that these results are sufficient to indicate that parasympathetic nervous system activity is not essential for PAR-2-mediated salivary secretion.

As shown in Fig. 3, we found that the composition of SLIGRL-OH-induced saliva was similar to that of mAChR activation-induced saliva; amylase activity in concentration and total protein concentration in secreted saliva induced by SLIGRL-OH or pilocarpine were much lower than those induced by isoproterenol, and protein concentration in SLIGRL-OH-induced saliva was comparable to that of pilocarpine-induced saliva. However the significant difference in total amylase secretion between SLIGRL-OH stimulation and pilocarpine stimulation demonstrates the higher activity

of pilocarpine to induce salivary secretion and that the intracellular signaling of mAChR and PAR-2 is not completely the same. From these results, we consider that stimulation with SLIGRL-OH induces fluid secretion rather than protein secretion, which is mainly induced by β-adrenergic stimulation (Slomiany et al., 1992), although some amount of amylase can be secreted as reported previously (Kawabata et al., 2000b, 2002b). The results also indicate that sympathetic nervous activity is not involved in PAR-2-mediated salivary secretion.

PAR-2 activation induces $[Ca^{2+}]_i$ increase in guinea pig tracheal epithelial cells (Oshiro et al., 2002), rat longitudinal muscle cells (Mule et al., 2002), and some cell lines (Kawabata et al., 2004a) or activates phospholipase C in longitudinal muscle (Mule et al., 2002). Considering these studies, PAR-2, as with M_1, M_3 and M_5, is likely to be coupled to $G_q/_{11}$ and increase $[Ca^{2+}]_i$ in salivary glands. Therefore, in the present study, we investigated $[Ca^{2+}]_i$ changes induced by SLIGRL-OH using enzymatically dispersed SMG cells and found that SLIGRL-OH induced dose-dependent $[Ca^{2+}]_i$ increase in the SMG acinar cells. The $[Ca^{2+}]_i$ increase was mediated by PAR-2, because this $[Ca^{2+}]_i$ increase was abolished in PAR-2KO acinar cells. Because $[Ca^{2+}]_i$ increase in acinar cells triggers fluid secretion in salivary glands, the above results indicate that direct activation in the salivary glands to evoke $[Ca^{2+}]_i$ increase in acinar cells causes PAR-2-mediated salivary secretion. As shown in a previous report (Nakamura et al., 2004), activation of mAChRs also induced $[Ca^{2+}]_i$ increases in the SMG cells. Taken together with the composition of saliva, PAR-2 mediates salivary secretion by a Ca^{2+}-dependent mechanism that is similar to mAChRs-mediated salivary secretion.

It is interesting that the total amount of SLIGRL-OH-induced saliva standardized by body weight in M_1/M_3KO mice was twice as large as that in WT mice. The small body size of mice lacking M_3 receptors (Matsui et al., 2000) is unlikely to result in the apparent salivary increase, because significant difference was not detected between the body weights of the mice used, and isoproterenol-induced salivary secretion standardized by body weight was similar among all of the groups tested (Fig. 2f). Rather, it is likely that some compensatory mechanism involving PAR-2, but not the β-adrenergic system, emerged in the salivary glands. Interestingly, we detected significant increase in the SLIGRL-OH-induced $[Ca^{2+}]_i$ response at 300 μM between WT and M_3KO mice or WT and M_1/M_3KO mice (Fig. 4e), showing the enhancement of PAR-2-mediated $[Ca^{2+}]_i$ increase in the M_3-deficient SMG. This enhanced $[Ca^{2+}]_i$ increase presumably contributes to the increased salivary secretion. PAR-2 expression was analyzed using reverse transcription-polymerase chain reaction for the mechanism of this increased salivary secretion and $[Ca^{2+}]_i$ increase; however, up-regulation of PAR-2 expression was not detected in M_1/M_3KO mice (data not shown). Some functional analysis may be needed to elucidate this mechanism. In PAR-2KO mice, a smaller $[Ca^{2+}]_i$ increase was detected than that in WT mice with 30 μM CCh, whereas a similar volume of saliva was secreted in PAR-2KO and WT mice with 5 mg/kg pilocarpine. So far, we do not know the clear reason for this discrepancy in the in vitro and in vivo response; therefore, further study is needed regarding this problem. We demonstrated PAR-2 distribution in the submandibular glands using Ca^{2+} imaging in WT mice and β-galactosidase staining in PAR-2KO mice in which the β-galactosidase gene was inserted downstream of the PAR-2 promoter instead of the PAR-2 gene. Although it is reported that PAR-2 was expressed throughout the parotid acini and pancreatic acini in rats (Kawabata et al., 2002b), our results revealed that PAR-2 is expressed in a heterogeneously scattered fashion in the mouse SMG. This distribution pattern is similar to that of the M_1-subtype and different from the ubiquitous expression of M_3 in the SMG acinar cells (Nakamura et al., 2004). This is the first demonstration of the distribution pattern of PAR-2 in the salivary glands that presumably accounts for the lower productivity of saliva by PAR-2 stimulation than that by mAChR stimulation. Some ductal cells expressed PAR-2, as well as acinar cells, in the β-galactosidase staining (Fig. 5c). Large ducts were removed in the SMG cell preparation for Ca^{2+} imaging; however, small ductal cells may have remained in the dispersed SMG, but those ductal cells can not be distinguished under microscopy. So far, the difference in the PAR-2 roles in acinar cells and ductal cells is still unclear.

The present study demonstrates that SLIGRL-OH directly activates PAR-2 in the salivary gland and induces $[Ca^{2+}]_i$ increase and salivary secretion without mediation via M_1 and M_3 subtypes. However, it remains under question whether and how PAR-2 is activated in the salivary glands under physiological conditions. It was reported that nanomolar concentration of trypsin cleaves and activates PAR-2 and that pancreatic trypsin may be capable of activating PAR-2 in some tissues (Dery et al., 1998). In addition to pancreatic trypsin, other trypsin-like enzymes can activate PAR-2: trypsinogen-2 in endothelial cells (Koshikawa et al., 1997) and mast cell tryptase (Corvera et al., 1997; Molino et al., 1997). Coagulation factors VII and X (Camerer et al., 1996; Belting et al., 2004) are reported as candidates of PAR-2 activators. Trypsin-like esteroproteases that were previously reported to be present in the mouse SMG (Takuma and Kumegawa, 1981; Takuma et al., 1985) may be a PAR-2 activator candidate. Further studies are needed to understand the physiological activation and inhibition mechanism of PAR-2 in salivary secretion.

There are still some problems to be solved, such as the rapid decline of salivary secretion induction following administration of SLIGRL-OH, the small volume of salivary secretion (less than 25% than the secretion by pilocarpine), and possible side effects because of widespread distribution of PAR-2 in many tissues. However, potent and metabolically stable agonists can induce larger salivary secretion as described in our results and another report (Kawabata et al., 2004a), and facilitation of fluid secretion is important for relief of xerostomia from a clinical point of view, even if the induced secretion volume is small. Furthermore, activation of PAR-2 may be favorable especially for the treatment of SS patients whose salivary secretion is inhibited by antimuscarinic antibodies (Dawson et al., 2006). Therefore, our present data demonstrate PAR-2 to be a potential drug target for patients who suffer from exocrine dysfunction, particularly those resulting from deficiency of functional cholinergic activation.

Acknowledgments

We thank Dr. Naohiro Saito for supplying the PAR-2KO mice, Roger E. Morgan for helpful comments and critical reading of the